REPORT NO.
TDR-930(2119)TR-2

The Kinetics of Ionization Processes in Gases

DECEMBER 1961

Prepared by H. MYERS

Prepared for DEPUTY COMMANDER AEROSPACE SYSTEMS
AIR FORCE SYSTEMS COMMAND
UNITED STATES AIR FORCE
Inglewood, California

AEROSPACE CORPORATI
CONTRACT NO. AF 04(647)-

Report Number
TDR-930(2119)TR-2

THE KINETICS OF IONIZATION PROCESSES IN GASES

by

Howard Myers

AEROSPACE CORPORATION
El Segundo, California

Contract No. AF 04(647)-930

December 1961

Prepared for

DEPUTY COMMANDER AEROSPACE SYSTEMS
AIR FORCE SYSTEMS COMMAND
UNITED STATES AIR FORCE
Inglewood, California

Report Number
TDR-930(2119)TR-2

THE KINETICS OF IONIZATION PROCESSES IN GASES

Prepared by Howard Myers
H. Myers
Aerodynamics and Propulsion
Research Laboratory

Approved by R. A. Hartunian
R. A. Hartunian, Head
Aerophysics Department

AEROSPACE CORPORATION
El Segundo, California

ABSTRACT

Currently available knowledge of the kinetics of ionization is presented. The production of ionization is covered by a description of electrical discharges in gases, including direct and alternating current discharges. Photoionization and ionization by shock waves are described. The measurement of ionization includes a description of electrostatic probes, microwave probing signals, mass spectrometer probe and shock tubes. Photoionization instrumentation is described. Results of kinetic investigations are presented and the ionization processes occurring in the atmosphere are analyzed.

CONTENTS

CONTENTS (continued)

SECTION I

INTRODUCTION

Electrical discharges in gases were first produced in the laboratory a century ago. In the intervening years the properties of ionized gases have become increasingly familiar. Nevertheless, knowledge of the mechanisms by which ionization is produced and destroyed within gases is still rather limited. This circumstance arises from the lack of data on the rates of ionization processes for the testing of theory. In order to obtain meaningful kinetic data, uniform ionized gases with well defined properties are required. This requirement was not usually met in electrical discharges. Therefore, until recently, measurements in the kinetics of ionization were made, not in the laboratory, but rather in the ionosphere. Indeed, observations on the behavior of the ionosphere continues to be the primary stimulus for the theoretical analysis of electron-ion recombination.

With the development of microwave methods and shock tubes as tools for basic physics research during the last decade, the study of ionization kinetics in the laboratory has been pursued vigorously. Analysis of the interaction of microwaves and free electrons has been particularly valuable in providing direct methods of measuring electron densities. Sufficient experience is now available with these new techniques to exploit them fully in a laboratory program of ionization research.

This study attempts to present our present knowledge of the kinetics of ionization in a systematic manner and was compiled with a twofold purpose: Firstly, to provide a collection of the available data for those who have a need for the information in their own researches (e.g. in the fluid dynamics of ionized gases). Secondly, to form the basis of a theoretical and experimental program of ionization research within the Aerophysics Department of the Aerospace Corporation.

SECTION II

PRODUCTION OF IONIZATION

A. Electrical Discharges in Gases

1. Direct Current Discharges[1, 2]

An electrical discharge is usually built up in a gas by the ionizing collisions of electrons and proceeds as a transient discharge until a self-sustaining mechanism is established. The various phases that arise in a discharge as the dc potential is changed are illustrated in Figure 1. The two most important processes are the glow discharge and the arc.

Glow and arc discharges are differentiated from one another by the mechanisms which create them. A glow discharge maintains itself by means of the secondary electrons which are liberated by the impact of positive ions on the cathode. If a single electron on leaving the cathode and passing to the anode creates n ion pairs, then the n positive ions must liberate at least one electron from the cathode for a self-sustaining discharge to be established. Usually the glow discharge is encountered at low pressures ($<$ 20 cm Hg) and low currents (10^{-3} to 1 amp), but high potentials of 100 to 400 volts are required for the positive ion mechanism to be effective. Glows are characterized by nonuniformity of their light emission. The luminous and dark regions arise from variations of local space charge conditions.

In arc discharges, on the other hand, the cathode emission is largely due to mechanisms other than positive ion bombardment. The predominant source of electrons is thermionic emission from the cathode. The potential difference across the electrodes is not required to be as large as for a glow discharge, and the discharge tends to be more uniform between cathode and anode. Unless the cathode is heated by external means, there will be a transition from a glow to an arc after the voltage is

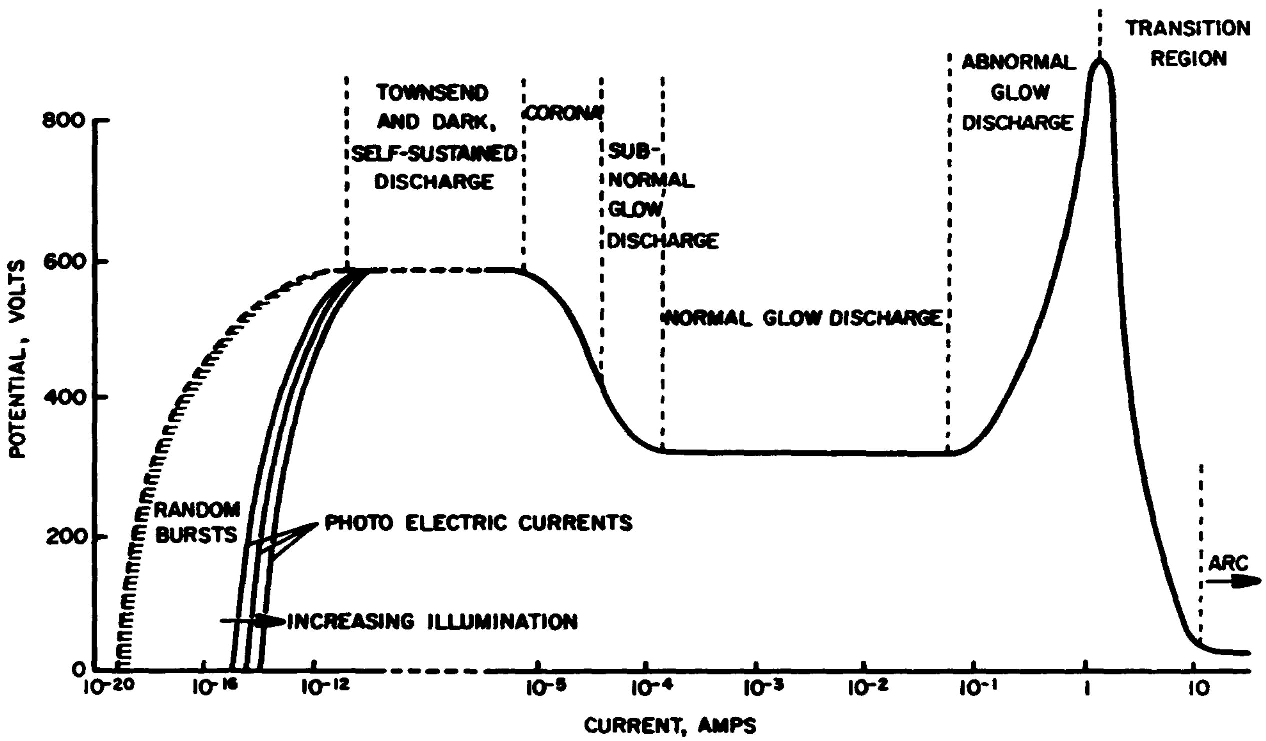

Figure 1. The Various Phases of a Direct Current Discharge

initially applied to the discharge tube. The role of processes such as high pressure glow discharges, glow-arc transition, and sparks in the preliminary stages of the arc discharge has not yet been fully determined.

2. Alternating Current Discharges[3,4].

The ionization processes that take place in a gas subjected to alternating electric fields differ from those in dc fields. The periodic reversal of field direction tends to prevent the charged particles from being swept out of the gas onto the walls and electrodes. Since ionization losses are reduced, a self-sustained discharge can be produced by quite low field strengths. In these circumstances secondary processes at the electrodes are not required for breakdown. Furthermore, secondary electrons produced along the walls of the vessel will contribute to the growth of the discharge only if they are emitted when the field is in a favorable direction: An ac discharge can be excited by means of external electrodes; the resultant electrodeless discharge can differ from that produced with internal electrodes. Lastly, ac discharges can be maintained in insulating vessels, and the drift of charged particles to the walls sets up static fields which can determine the density of ionization in the gas.

Low Pressure Discharges

At such low pressures ($< 10^{-2}$ mm Hg) that the mean free path is greater than the dimensions of the vessel, the collisions of electrons with the walls are more frequent than with gas molecules. Consequently, secondary processes of the walls control breakdown. The electrons will multiply initially only if they move back and forth between the walls in resonance with the field and strike the walls hard enough to eject secondary electrons. The starting potential is, therefore, determined by the material of the electrodes (or the walls in an electrodeless discharge) and the geometry of the vessel; it is independent of the nature of the gas. The properties of the fully developed discharge, however, depend on the gas and hardly at all on the walls.

At pressures where the mean free path is appreciably less than the dimensions of the vessel, the behavior of the discharge depends on the relation between the collision frequency ν_c and the frequency f of the applied field. When $\nu_c >> f$, the electrons make many collisions for each oscillation of the field, and drift as a cloud in phase with the field. When $\nu_c << f$, the electrons make many oscillations between collisions, and a cloud of electrons would appear stationary, spreading outward only by diffusion. In this situation the condition for producing a discharge is that on the average each electron must liberate one new electron in the time it takes to diffuse to the walls.

The inter-relation between collision frequency and field frequency is illustrated by the shape of a typical breakdown voltage vs pressure curve. As the pressure is decreased the voltage required for breakdown first decreases and then increases. In the low pressure region (1-10 mm Hg) the breakdown field must increase with decreasing pressure in order to compensate for the decreasing efficiency of energy transfer from the field to the electrons. Since in an alternating field the electrons oscillate out of phase with the field, they absorb no energy from it; therefore, the electrons gain energy only from the gas molecules. Thus, to maintain the ionization rate as the pressure is reduced, the field strength must be increased. In the high pressure region (100 to 1000 mm Hg), the electron energy gain per path length is proportional to the mean free path at constant E field. With increasing pressure the field must be increased inversely proportionally to the mean free path, or directly proportionally to the pressure. The minimum in the voltage-pressure curve corresponds essentially to the point where $f = \nu_c$.

Microwave Pulse Discharge

The conditions for initiating breakdown of a gas by a microwave pulse differ from those of a diffusion controlled breakdown. In the latter, breakdown occurs when a relatively slow growth of ionization just exceeds the rate of loss. With a pulsed field breakdown can occur only if the ion and electron density grows so rapidly that the discharge reaches a steady state during the time the pulse is applied. The breakdown condition in the noble gases is a field strong enough to build up a certain critical number of ion pairs within the duration of the pulse. For diatomic gases the breakdown field does not vary with the pulse time; rather breakdown occurs when a few favorable collisions lead immediately to instability and breakdown. This condition could arise if a group of oscillating electrons sweeping repeatedly through a small volume of gas produce a concentration of excited molecules, and then ionize them in subsequent oscillations.

B. Photoionization[5]

Ionization occurs in a gas when a photon of energy $h\nu$ equal to or greater than the ionization potential is absorbed by an atom or molecule. The electron that is ejected has kinetic energy equal to the difference between the photon energy and the ionization potential. The critical wave length (in Å) for ionization is given by $\lambda = 12{,}400/V_i$ where V_i, the ionization potential, is in electron volts. Thus, 2000-3000Å light will ionize alkali metal vapors and 500Å light will ionize the inert and molecular gases. The probability of photoionization is at a maximum when $h\nu - eV_i$ is small ($\sim$ 0.1 to 1 ev) and decreases with decreasing wavelength.

C. Ionization by Shock Waves

A transitory state of ionization can be induced in a gas by the passage of a sufficiently strong shock wave. In the usual shock tube arrangement, a volume of gas at high pressure is separated from a gas at low pressure by a thin diaphragm which when ruptured allows the compressed gas to rush into the rarefied region. A discontinuous change in pressure and density across the shock front occurs; the zone of gas immediately behind the shock front is a region of high gas density, pressure, and temperature. At some distance behind the front thermal equilibrium is re-established at a high temperature. For example, a shock front moving at Mach 18 through argon initially at room temperature and 10 mm Hg pressure produces an equilibrium temperature of 14,000°K and a degree of ionization of 25 percent.

A considerably greater degree of ionization is obtained from magnetically driven shock waves.[6] Through the use of this technique, shock velocities in excess of Mach 50 are attainable; however, the state of the plasmas obtained cannot be specified with sufficient accuracy to be useful immediately in the study of the kinetics of ionization.

REFERENCES

1. G. Francis, "Glow Discharge of Low Pressure," Handbuch der Physik, Bd. 22, s. 53, Springer-Verlag, Berlin 1956.

2. J. M. Meek and J. D. Craggs, "Electrical Breakdown of Gases," Calrendon Press, Oxford 1953.

3. G. Francis, "Ionization Phenomena in Gases," Ch. 4, Butterworths Scientific Publications, London 1960.

4. S. C. Brown, "Breakdown of Gases: Alternating and High Frequency Fields," Handbuch der Physik, Bd. 22, s. 531, Springer-Verlag, Berlin 1956.

5. G. L. Weissler, "Photoionization in Gases and Photoelectric Emission from Solids," Handbuch der Physik, Bd. 21, s. 304, Springer-Verlag, Berlin 1956.

6. A. C. Kolb, Phys. Rev. 107, 345 (1957).

SECTION III

MEASUREMENT OF IONIZATION

A. Electrostatic Probes

Inherently, the simplest device for measuring ionization densities is the electrostatic probe. The use of electrical probes for the study of ionized gases began with Langmuir's research in the nineteen-twenties. Although electrical probes have undergone extensive development their response to plasmas is not yet fully understood. In principle the plasma potential can be determined by measuring the potential acquired by an isolated probe placed in the gas. However, large errors in measurements of the potential are found to occur when a probe is inserted into a region where either positive ions or electrons predominate.

The Langmuir technique[1] consists of observing the current drawn to the probe as its potential is varied from strongly negative to positive relative to the plasma potential. When the probe is strongly negative all electrons are repelled; the positive ions are attracted and form an ion sheath on the surface of the probe. The current to the probe is limited by the space charge of the ions, and is constant. If the probe is made less negative some of the faster electrons can reach the probe surface, specifically those having a velocity perpendicular to the probe such that $1/2\ mv^2 \geq eV$. Provided the probe is kept negative, the velocity distribution of the electrons can be deduced from the variation of the probe current with potential. This variation has a special form if the distribution is Maxwellian: the electron current density j_e is given by

$$j_e = n_e e \sqrt{\frac{kT_e}{2\pi m_e}} \exp(-eV/kT_e) \qquad (1)$$

where

n_e = electron density

e = electron charge

k = Boltzmann constant

T_e = electron temperature

m_e = electron mass

The logarithm of the current density plotted against the probe potential yields a straight line from whose slope the electron temperature is determined. When the probe potential is made equal to the plasma potential, the positive ion sheath disappears; at more positive potentials it is replaced by a much thicker sheath of electrons. At $V_{probe} = V_{plasma}$, the net voltage V is zero and the formula for the current density reduces to

$$je = n_e e \sqrt{kT_e/2\pi m_e} \tag{2}$$

With T_e previously determined from the slope of the curve, the electron density n_e is found. Hence, the significant properties of a plasma in steady state can be deduced by systematically altering the electrical potential of the probe.

The probe method is subject to a number of limitations; when these difficulties are recognized, the interpretation of experimental data can be adjusted to take them into account.[2] The Langmuir procedure must be modified to be applicable to transistory plasmas, as arise in shock waves, where the charges removed by the ion currents are not replaced. A technique developed for decaying plasmas consists of two identical probes placed a short distance apart in the plasma. A small and reversible potential is applied between them, but the whole system is unconnected to any fixed source of potential. One measures the current flowing in the circuit as the differential voltage is varied. The theory for these probes differs from that of Langmuir's probe and is based on Kirchoff's current law, which requires that the total net current flowing to the circuit from the plasma is zero. This type of probe can be used directly to measure the potential of the plasma; a direct measurement is not possible with the conventional probe.[3]

B. Microwave Probing Signals

In studies of the decay of ionization in plasmas, the ionization can be produced under experimentally convenient circumstances by means of a pulsed high-frequency discharge. Once the plasma is established and the applied field switched off, the ions and electrons disappear by a rate characteristic of the process by which they are removed, be it by diffusion, electron-ion recombination, or attachment of electrons to neutral species.

The method most commonly used to measure the rate of electron disappearance is based on the conductivity of the plasma in a weak microwave field, used as a probing signal.[4] The motion of the electrons in the plasma is out of phase with the applied field; therefore, the conductivity is complex. The real and imaginary parts of the conductivity correspond to the current in phase and at 90° to the applied field, respectively. The former absorbs power and depends on both the electron density n_e and the collision frequency ν_c; the latter absorbs no power and, provided the collision frequency is very much less than the frequency of the field, depends on n_e but not on ν_c.

In practice, measurements of electron decay rates are usually made on plasmas contained in a microwave cavity. The experimental arrangement is illustrated in Figure 2. The ionization is produced by a pulsed microwave field, and changes in the resonance frequency and the Q of the cavity are measured during decay. The change in the angular resonance frequency, ω, of the cavity caused by electron currents in the plasma is given by Slater[5] as

$$\frac{\omega - \omega_o}{\omega_o} = - \frac{1}{2\omega_o} \int_V \sigma_i E^2 \, dV \Big/ \int_V E^2 \, dV \qquad (3)$$

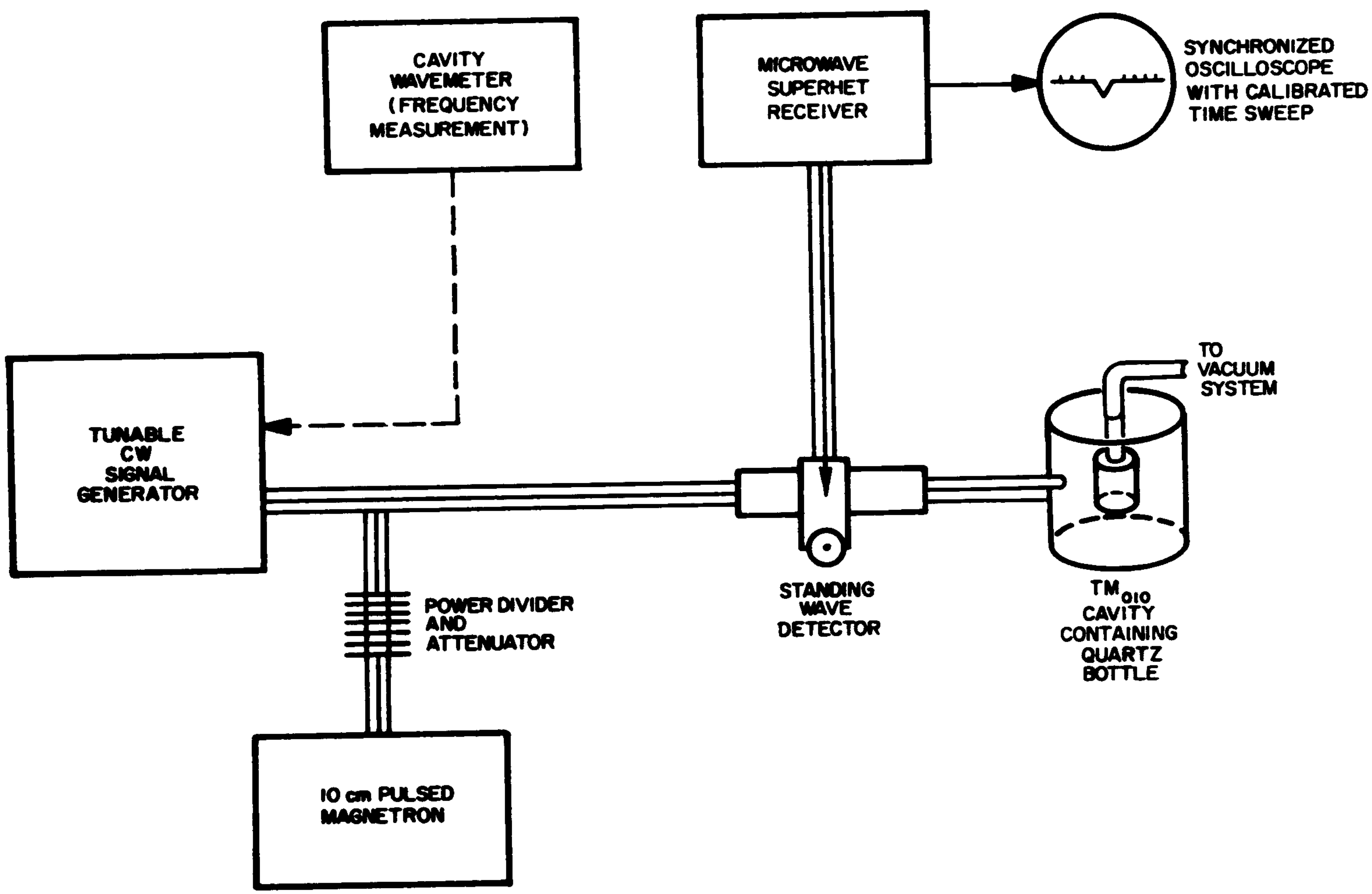

Figure 2. Block Diagram of Microwave Cavity Apparatus for Studying Electron Density Decays in Afterglows

Substituting into this expression Margenau's formula for the imaginary part of the conductivity σ_i ,[6]

$$\sigma_i = -\frac{n_e e^2}{m_e \omega}\left[1-(\nu_c/\omega)^2\right] \tag{4}$$

and integrating over the volume of the cavity, the relation between $\Delta\omega$ and n_e is obtained:

$$\frac{\Delta\omega}{\omega_o} = 2\pi\frac{n_e e^2}{m_e \omega_o^2}\,\frac{1}{\left[1+(\nu_c/\omega)^2\right]}\,G \approx 2\pi\frac{n_e e^2}{m_e \omega_o^2}\,G \tag{5}$$

(G is a geometrical factor depending on the distribution of the plasma and the field in space.) The change in the Q of the cavity is given by

$$\frac{1}{Q} - \frac{1}{Q_o} = 4\pi\frac{n_e e^2}{m_e \omega_o^2}\cdot\frac{\nu_c/\omega}{1+(\nu_c/\omega)^2} \quad . \tag{6}$$

To determine the rate of electron disappearance a weak continuous signal is fed into the cavity. The time sequence of the electron density is shown in Figure 3. As the electron density decays and reaches a value such that the resonance frequency of the cavity (f_{cav}) is equal to the signal frequency ($f_{s,1}$), there is at that instant (t_1) a maximum in the absorption of the signal by the cavity. By repeating the sequence of discharge and decay using different probing signal frequencies the rate of electron density decay is established.

In the original application of microwave techniques to afterglows in plasmas, a study of diffusion in helium by Brown and Biondi,[4] the gas was ionized with a 250 μsec pulse from a 10 cm wavelength magnetron. During the pulse a steady-state charge density of 10^{10} to 10^{11} ions/cm^3 was produced. The magnetron was then shut off for 11 milliseconds and the change

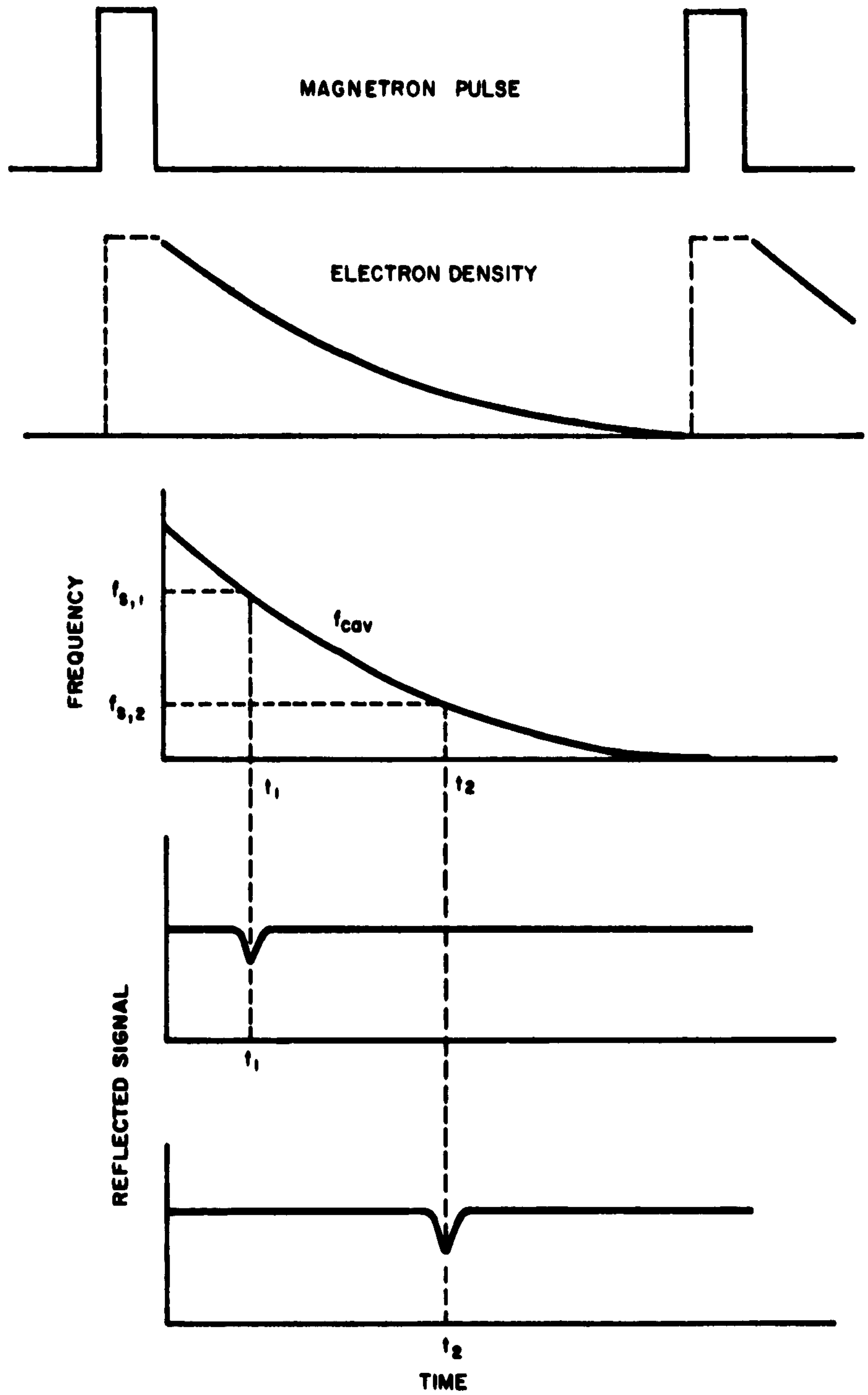

Figure 3. Time Sequence in Electron Density Measurements in Microwave Cavities

in electron density was measured in this interval. A block diagram of their microwave apparatus is shown in Figure 2. A full description of the experimental technique is given by Biondi in reference 7.

The microwave cavity technique has proved to be very fruitful and has been extensively applied during the last decade. The capability of the method is enhanced by supplementing the microwave measurements with simultaneous spectroscopic observations. Along with the growing use of microwaves, the method has been subjected to careful scrutiny. In particular, Persson[8] has examined the limitation imposed on the measurement of electron density by the use of Slater's formula. The simplifying assumptions of the derivation, particularly that the current due to the motion of the electrons is small compared with the displacement current, restrict accurate estimates of electron density to the range of 5×10^7 to 5×10^9 electrons/cm^3. The upper limit to the measurement of electron density is set by the plasma resonance due to the macroscopic polarization of the plasma. In addition, as the electron density increases, the space charge field becomes large inducing other modes of excitation in the cavity. The macroscopic electric polarization can be eliminated and the overlapping modes suppressed by designing the cavity so that the probing microwave field and the plasma have rotational symmetry around the same axis. The electric polarization limit and available range is thereby extended to 5×10^{10} electrons/cm^3 at 3000 mc/sec. Persson further estimates that decreasing the frequency of the probing signal from 3000 mc/sec to 1 mc/sec and measuring the Q or electron losses of the plasma in a properly designed solenoid instead of a cavity would permit accurate measurements of electron density up to 10^{16} electrons/cm^3.

C. Mass Spectrometer Probe

A miniature time-resolving mass spectrometer has been developed by Boyd[9,10] for the study of electrical discharges. The spectrometer is designed to serve as a movable probe capable of being inserted into the discharge. The device is essentially a tiny linear accelerator and, therefore, there is no external magnetic field present which might disturb the afterglow. The mass selection is based on the dependence of the ion energy gain upon the time-of-flight along the ion path. An initial dc accelerating field converts the mass spectrum to a velocity spectrum. For kinetic investigations the variation of the resultant ion current with time provides a measure of the time variation of specific ion concentrations in the afterglow.

The instrument has been used extensively by Boyd in dc discharge studies and by Sayers in studies of the decay of afterglows.

D. Measurements in Shock Tubes

A number of techniques have been utilized in the measurement of electron densities behind shock waves. Of greatest value to the task of determining the specific mechanism of ionization for a particular system are data on the instantaneous change in electron density. Not all the techniques discussed below are capable of providing this information; some methods can only determine the time required by the system to attain thermodynamic equilibrium.

Several methods have been developed in an attempt to avoid the difficulties which arise with electrostatic probes in correlating probe potentials and electron densities. Two of these methods are based on the electromagnetic properties of an ionized fluid. The first is a magnetic induction method of determining electrical conductivity in the shock wave.[11] An axially symmetric magnetic diode field is set up in the shock tube. The passage of the ionized shock-heated gas through the magnetic field displaces the magnetic lines of force. By measuring this magnetic field displacement through a nearby coil and comparing the signal with that produced by a known conductor, the electrical conductivity can be deduced.

The second method involves the interaction between the plasma and microwave radiation. In one application of microwave techniques the attenuation of a microwave beam transmitted through the ionized gas is measured and the extinction coefficient determined.[12] If the electrical conductivity of the gas is measured simultaneously (by magnetic induction, for example) the values of the conductivity and extinction coefficient may be combined through classical dispersion theory[13] to obtain the electron collision frequency of the plasma. The electron density in turn is obtained from the collision frequency and the conductivity:

$$n_e = \frac{m_e}{e^2} \sigma \nu_c \tag{7}$$

A more direct determination of electron density is provided by a measurement of microwave reflectance rather than absorption[14]. It is assumed that at the frequencies employed the plasma behaves as a pure dielectric, and the terminal impedance of a microwave probe is measured. The probe consists of a section of rectangular waveguide terminating in a half-wave dielectric window. The probe is inserted into the shocktube and oriented normal to the flow. The terminal impedance of the probe is measured in terms of a power reflection coefficient, which in turn is related to the electron density. For this procedure to be applicable, the electron density must not exceed a limiting value corresponding to plasma resonance at the frequency of the probing signal used. The critical electron density is given by the formula

$$n^*_e = \frac{\pi m_e}{e^2} f^2 = 1.24 \times 10^{10} f^2 \tag{8}$$

where the frequency f is expressed in kilomegacycles/sec. At this electron density the dielectric constant falls to zero and total reflection results.

The microwave power reflection coefficient R is determined from the ratio of incident to reflected power

$$|R|^2 = P_r/P_i \tag{9}$$

The relation between the power reflection coefficient to the dielectric constant of the plasma is complex and is dependent on the geometry of the apparatus; however, the simple plane wave formula

$$|R|^2 = \left|\frac{1 - \sqrt{\epsilon}}{1 + \sqrt{\epsilon}}\right|^2 \tag{10}$$

serves as a good approximation. Finally, the electron density is related to the dielectric constant

$$\epsilon = 1 - \frac{n_e}{n_e^*} \quad , \tag{11}$$

so that for a given microwave frequency the power reflection coefficient provides a direct measure of the electron density,

$$R^2 = \left|\frac{1 - \sqrt{1 - (n_e/n_e^*)}}{1 + \sqrt{1 - (n_e/n_e^*)}}\right|^2 \quad . \tag{12}$$

A comparison of electron densities deduced from probes of different frequencies ($10 < f < 35$ kilomegacycles/sec) indicates that the uncertainty in using the plane wave approximation is no greater than the experimental scatter from other sources.

A microwave absorption determination of electron densities has been reported recently which involves passing microwaves longitudinally down the shock tube.[15] The shock tube itself is made from rectangular waveguide. The microwave source is located behind the high pressure section and a crystal diode detector is mounted behind the low pressure section. The electron density is determined from the expression for microwave absorptivity D in a rectangular waveguide,

$$D = \log I_o/I = \beta z n_e \tag{13}$$

where I is the intensity of radiation, β is the absorption coefficient, and z is the path length. The magnitude of D gives the total number of electrons in the shock tube; when D is a function of n_e, it is dependent on both the total number of electrons and their distribution in space. Therefore, the measuring technique is restricted in its application to electron densities at which β is a constant.

Compared to probes and to spectroscopic devices the electromagnetic techniques suffer from relatively poor spatial resolution. The spatial resolution of magnetic induction is limited by the diameter of the sensing coil and the effective width of the magnetic field. Microwave reflection is limited by the wavelength employed.

In addition to the methods described above several optical techniques have been used to estimate the degree of ionization in shock waves. Beginning with the initial observation that a highly luminous region is associated with the shock front at high shock strengths,[16] there has been a progressive development of high-speed, time-resolved spectroscopy. In the early studies it was not possible to make spectrographs of the luminous region itself because of the short exposure time associated with high shock velocities. As experimental techniques improved, it was found that the luminous radiation of the shock front could be resolved and analyzed spectroscopically.

The first spectrograms of shock waves in argon revealed that the observed luninosity was due to continuum radiation. The development of a rotating drum camera spectrograph which provided time resolution of about 1 μsec furnished evidence that for Mach numbers above 10 thermodynamic equilibrium in argon is attained in the testing times available in the shock tube. By a further refinement of experimental techniques Petschek and Byron[17] were able to make direct measurements of the time required for shock-heated argon to reach equilibrium. In their study of ionization kinetics, the drum camera was supplemented by high-response time photomultipliers and oscilloscopes in order to measure the change in radiation intensity with time.

The techniques of optical interferometry also have been applied to the measurement of electron concentrations in shock-ionized gases.[18] The specific property that is measured in conventional interferometry is the phase index of refraction. In a strongly dispersive medium such as a plasma the group and phase indices of refraction are no longer identical. A change in the group index of refraction is revealed on an interferogram by a change in the position of the center of contrast of the interference fringes; a change in the phase index is revealed by a change in the location of a particular interference fringe representing a given order of interference.

The refractivity of the free electrons produces most of the refractivity of an ionized gas. The index of refraction for electrons is related to the plasma frequency and the angular frequency of the propagated light. The phase index of refraction is given to a good approximation by

$$\mu_p = 1 - \omega_p^2/2\omega^2 \qquad (14)$$

and the group index of refraction by

$$\mu_g = 1 + \omega_p^2/2\omega^2 \tag{15}$$

where the plasma frequency, ω_p is given by

$$\omega_p = (4\pi n_e e^2/m_e)^{1/2} \tag{16}$$

In terms of the observing wavelength,

$$\mu_p = 1 - 4.46 \times 10^{-14}\lambda^2 n_e$$

$$\mu_g = 1 + 4.46 \times 10^{-14}\lambda^2 n_e \tag{17}$$

where the wavelength λ is in centimeters.

The refractivity of the electrons is proportional to the square of the wavelength of observation; the refractivity of the other species present varies only slightly through the entire visible spectrum.

The large dispersion of the refractive index due to electrons suggests that measurements of the total index of refraction of the plasma at two wavelengths would permit a direct determination of the electron concentration. Alpher and White determined electron concentrations in shock-ionized argon by photographing the shock wave simultaniously through two different interference filters. Equilibrium electron densities in the range of 10^{16} to 10^{17} electrons/cm^3 were measured and the values agreed closely with those calculated from shock Rankine-Hugoniot relations. Interferometry, therefore, offers a method for analyzing plasmas at electron densities that are inaccessible to conventional microwave and probe techniques.

The interferograms provide a continuous record of shock-induced ionization. The relaxation process is strikingly portrayed in the interferograms and the relaxation time is directly measurable. Alpher and White have not to date attempted to interpret the detailed features of their interferograms in terms of the kinetics of ionization. One obstacle to such a project is that the lowest electron concentration observable in the interferograms is about 5×10^{16} electrons/cm^3, corresponding to less than one-tenth of an interference fringe shift. Consequently the initial stages of ionization are interferometrically invisible. Nevertheless, used in conjunction with other experimental techniques, the interferometer may prove to be a valuable device for the study of plasma kinetics.

E. Photoionization Instrumentation

The interaction between light and an absorbing medium is conveniently expressed in terms of an absorption coefficient . The reduction of intensity $-\Delta I$ of a monochromatic beam of light in going a distance Δx through the medium is given by

$$- \Delta I = \mu I \Delta x \quad . \tag{18}$$

Since μ is considered a property of the absorbing medium only,

$$I = I_o \exp (- \mu x) \tag{19}$$

The measurements at different temperatures and pressures all reduce to the same value of μ which is proportional only to the concentration η of the absorber, $\mu = \sigma n$. The proportionality constant σ has the dimensions of area and can be regarded as the cross section which a molecule presents to the incident radiation. If the gas is sufficiently rarefied so that the influences of intermolecular forces are negligible, the cross section is a characteristic property of the gas.

The complete determination of photoionization cross sections involves the estimation of the total absorption cross section from measured values of I_o/I and the path length, the measurement of the number of ions produced per second, the evaluation of the absolute value of I_o, and the number of photons per second impinging on the column of absorbing gas. Knowing the total absorption and the initial quanta available, one can calculate the number of photons removed from the light beam per second over a specific section of its path. By collecting the ions produced along this section and measuring the ion current, the ratio of ion current to photons absorbed yields the photoionization efficiency. This number multiplied by the total absorption cross section gives the photoionization cross section for the given wavelength. In principle, then the determination of photoionization cross sections is seemingly quite straightforward. Nevertheless the simultaneous measurement of absorption coefficients and photoionization efficiencies involve a number of technical difficulties. Until recently, therefore, most investigators confined themselves to measuring absorption coefficients alone.

The first quantitative values for photoionization cross sections were obtained by Mohler[19] for rhubidium and cesium vapors. The alkali metal vapors are particularly suitable to direct photoionization measurements because their low ionization potentials permit the use of quartz or fluoride optics. The initial results for the alkali metals were significantly improved by the efforts of Ditchburn[20] and his co-workers. In their experimental arrangement shown in Figure 4, the metallic vapors are contained in a heated absorption cell placed between the light source and the spectrograph. The radiation from a hydrogen glow discharge is passed through the absorption cell and impinges on the slit of a fluorite vacuum spectrograph. The absolute absorption cross sections of the alkali metals and of magnesium, calcium, indium and thallium have been obtained in this manner.

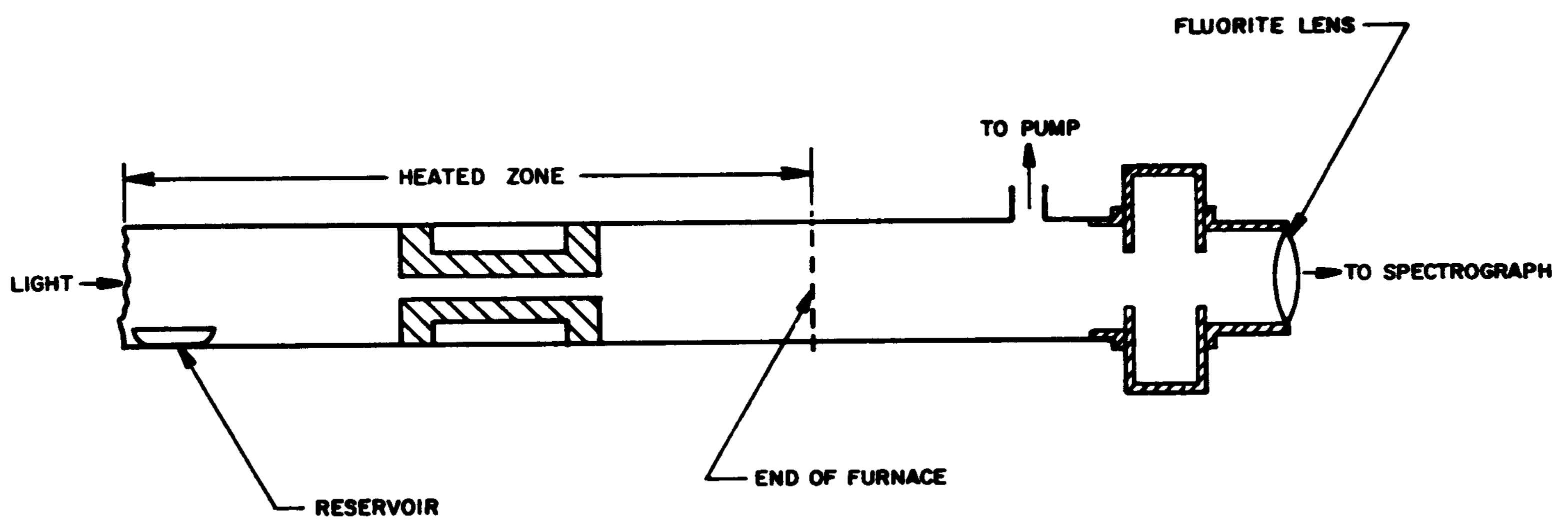

Figure 4. Heated Absorption Cell for the Photoionization of Metallic Vapors

For photoionization measurements below the lithium fluoride cutoff at 1050Å, a windowless grazing-incidence spectrograph, shown in Figure 5, has been designed by Weissler[21]. The gas to be studied fills the body of the spectrograph itself. The light source is a low pressure spark discharge which provides spark lines of sufficient intensity down to 200Å. The discharge carrier gas in the light source is prevented from contaminating the absorbing gas in the spectrograph by the insertion of a differential pumping chamber between the two sections. Another useful instrument for the study of the molecular gases is the normal incidence vacuum monochromator. In the instrument designed by Tousey[22] the relative intensities of the transmitted light is measured with a photomultiplier tube coated with sodium salicylate, a material which fluoresces in the vacuum ultraviolet. The light fluxes required by this instrument are several orders of magnitude smaller than in the spectrographs previously described. This feature is particularly valuable for absorption studies in gases which are sensitive to photochemical reactions.

Weissler[23] has recently developed an instrument for the simultaneous measurement of total absorption cross sections and photoionization efficiencies. In this device the light from a spark source illuminates the primary slit of a normal incidence grating vacuum monochromator where it is dispersed and focused on an exit slit. The absolute energy of the light beam is determined with a sensitive thermocouple located adjacent to the exit slit. Radiation of known wavelength and intensity passes through the exit slit into the experimental chamber, which contains the absorbing gas and three parallel plate ionization chambers arranged in tandem along the axis of the light beam. From the respective ion currents measured separately at the three collectors it is possible to obtain the total absorption cross section of the gas. The value of the cross section can be used to calculate the number of photons removed from the beam per second. The ratio of this number and the number of ions produced per second yields the photoionization efficiency.

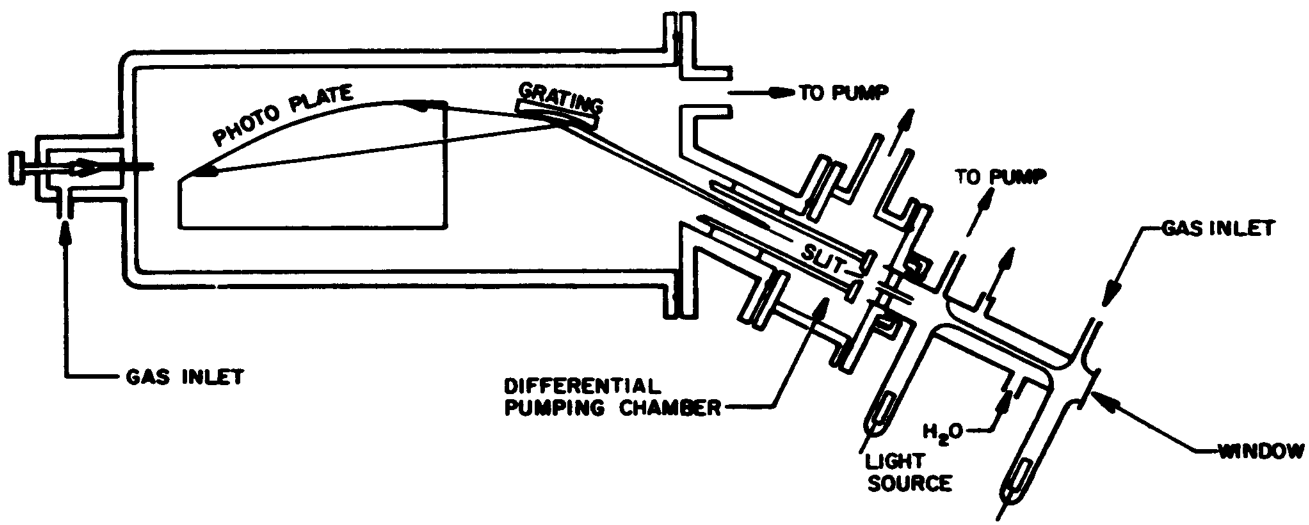

Figure 5. Windowless Grazing Incidence Vacuum Spectrograph

The photoionization cross section data obtained with a vacuum monochromator combined with an ion collector represent total cross sections without regard to the specific identity of the ions formed. Identification of the ion fragments produced by photon bombardment is accomplished by means of mass spectroscopy. The feasibility of combining a mass spectrometer with a vacuum monochromator was demonstrated by Inghram. Inghram's apparatus contained fluoride windows, which limited observations to above 1080Å. Weissler has devised a windowless monochromator mass spectrometer combination shown in Figure 6 which permits the study of photoionization studies down to 430Å. With this device Weissler's group analyzed a number of diatomic and triatomic gases and determined the relative yields of the various ion fragments.

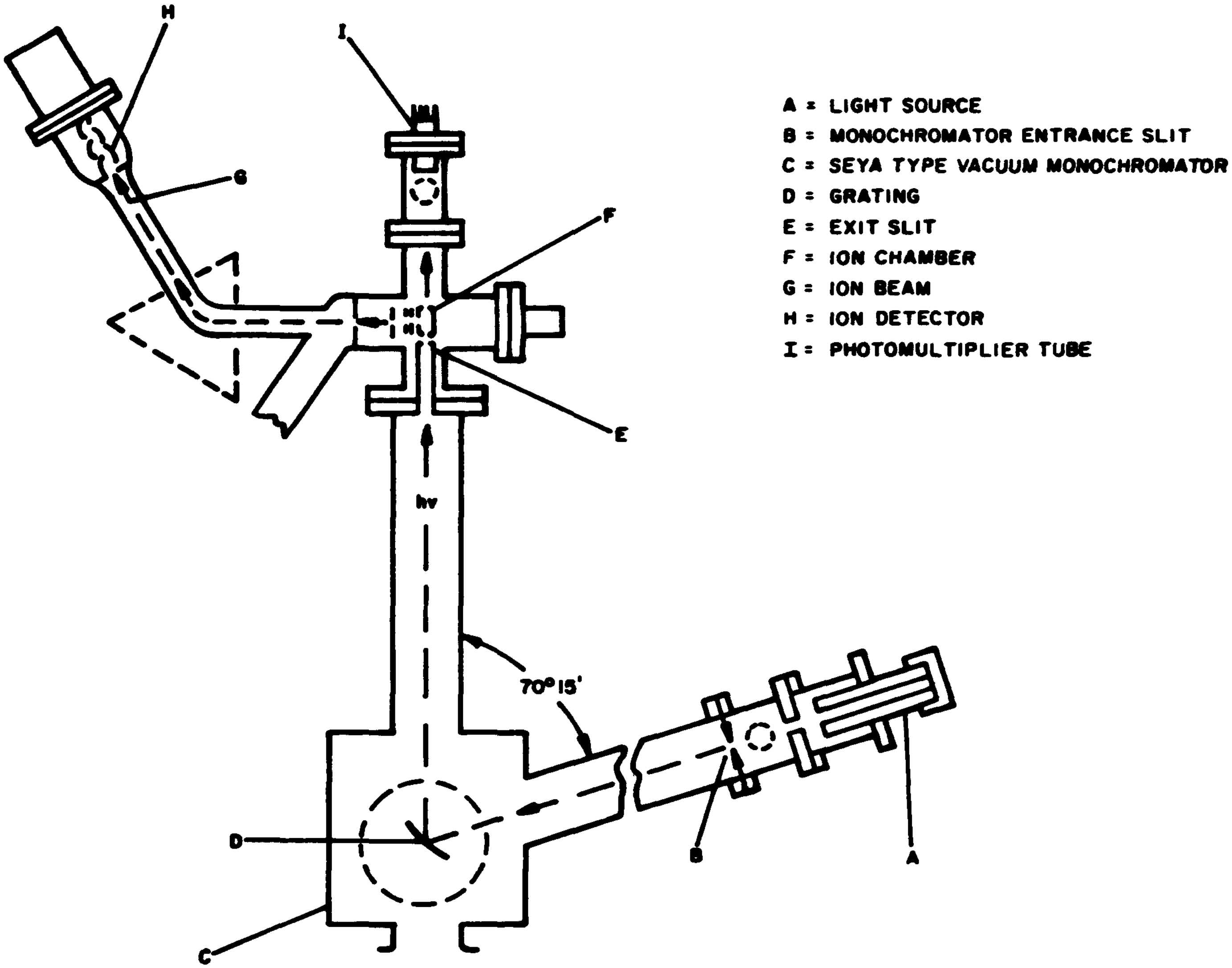

Figure 6. Windowless Vacuum Monochromator-Mass Spectrometer Combination for Identification of Ion Fragments Produced in Photoionization

REFERENCES

1. I. Langmuir and H. M. Mott-Smith, Gen. Elec. Rev 26, 731 (1923); 27, 449, 583, 616, 726, 810 (1924). I. Langmuir and K. T. Compton Rev. Mod. Phys. 3, 191-257 (1931).

2. R. L. F. Boyd, Proc. Roy Soc. A201 22 (1950); Proc. Phys. Soc. Lon. B64, 795 (1951).

3. E. O. Johnson and L. Malter, Phys. Rev. 80, 58 (1950).

4. M. A. Biondi and S. C. Brown, Phys. Rev. 75, 1700 (1949).

5. J. C. Slater, Rev. Mod. Phys. 18, 441 (1946).

6. H. Margenau, Phys. Rev. 69, 508 (1946).

7. M. A. Biondi, Rev. Sci. Instrum 22, 500 (1951).

8. K. B. Persson, Phys. Rev. 106, 191 (1957).

9. R. L. F. Boyd, Nature 165, 142 (1950); R. L. F. Boyd and D. Morris, Proc. Phys. Soc. Lon. A68, 1 (1955).

10. Similar devices are described by W. L. Kerr, J. of Electronics, 2, 189 (1956) and P. A. Redhead, Can. J. Res. 30, 1 (1952).

11. S. C. Lin, E. L. Resler, and A. R. Kantrowitz, J. Appl. Phys. 26, 95 (1955).

12. S. C. Lin, Avco-Everett Research Laboratory, Res. Dept. 33, June, 1958.

13. E. V. Appleton and F. W. Chapman, Proc. Phys. Soc. Lon. 44, 246 (1932).

14. S. C. Lin, Avco-Everett Research Laboratory, Res. Note 170, Dec. 1959.

15. H. S. Johnston and W. Kornegay. Trans, Fara. Soc. to be published.

16. E. L. Resler, S. C. Lin, and A. R. Kantrowitz, J. Appl. Phys. 23, 1390 (1952).

17. H. Petschek and S. Byron, Ann. Phys. (N. Y.) 1, 270 (1957).

18. R. A. Alpher and D. R. White, Phys. Fluids 2, 162 (1959).

19. F. L. Mohler and C. Boeckner, J. Res. Nat. Bur. Stand. 3, 303 (1929).

20. R. W. Ditchburn, P. J. Jutsum, G. V. Marr, Proc. Roy. Soc. A219, 89 (1953).

21. G. L. Weissler, PoLee and E. I. Mohr, J. Opt. Soc. Amer. 42, 84 (1952); PoLee, J Opt Soc. Amer. 45, 703, (1955).

22. R. Tousey, F. S. Johnson, J. Richardson and N. Tarau, J. Opt Soc. Amer. 41, 669 (1951).

23. N. Wainfan, W. C. Walker and G. L. Weissler, J. Appl. Phys., 24, 1318 (1953).

24. H. Hurzeler, M. G. Inghram and J. D. Morrison, J. Chem. Phys. 28, 76 (1958).

25. G. L. Weissler, Jar Samson, M. Ogawa, G. R. Cook, J. Opt. Soc. Amer. 49, 338 (1959).

SECTION IV

RESULTS OF KINETIC INVESTIGATIONS

A. Electron-Ion Recombination in Afterglows

The most extensive information on the rates of electron-ion recombination have come from microwave and spectroscopic observations of the afterglows of plasmas. When the field exciting the discharge is extinguished, the electron density decays according to the relation

$$\frac{\partial n_e}{\partial t} = - D_a \nabla^2 n_e - \alpha\, n_e n_+ - h\nu_a\, n_e \quad , \tag{20}$$

where it may be assumed that electrons are removed by ambipolar diffusion (D_a), recombination (α is the recombination coefficient and n_+ is the positive ion density), and attachment (h is the attachment probability and ν_a is the electron-molecule collision frequency). Experimental conditions are chosen so that one of the processes predominates: diffusion at low pressures or gas phase recombination at high pressures. The extent of electron attachment is governed primarily by the electron affinity of neutral species which are present in the plasma.

Ambipolar diffusion involves the simultaneous diffusion of electrons and positive ions in the presence of their own space charges. If diffusion is the dominant process, the solution of the rate equation, neglecting the terms describing the competing processes, leads to the exponential decay of n_e with time in several modes (i.e., different time constants). When the higher modes have died away and only the lowest order mode remains,

$$\frac{n_e}{n_{eo}} = \exp(-tD_a/L^2) = \exp(-t/\tau) \quad . \tag{21}$$

L is the characteristic diffusion length of the container. When only the lowest order mode remains, a plot of log n_e vs t gives a straight line of slope

$$\frac{1}{\tau} = D_a / L^2 \quad . \tag{22}$$

If electron-ion recombination predominates, it is assumed that n_e = n_t and the solution of the rate law is

$$\frac{1}{n_e} - \frac{1}{n_{eo}} = \alpha t \quad . \tag{23}$$

Hence, a plot of $1/n$ vs t is linear with slope.

If attachment is the only important process, then

$$n_e = n_{eo} \exp(-h\nu_a t) \quad , \tag{24}$$

and the slope of the log n_e vs t curve determines $h\nu_a$. Attachment may be distinguished from diffusion by the dependence on pressure, since ν_a is directly proportional to pressure, while D_a is inversely proportional to pressure.

1. Rare Gases

The original application of microwave techniques by Brown and Biondi[1] concerned a study of ambipolar diffusion in helium. However, in the course of their work, the investigators determined the rate constant for gas phase recombination in order to correct for recombination in their diffusion measurements. The observed value for ion-electron recombination was unexpectedly high, $\alpha = 1.7 \times 10^{-8}$ cm^3/ion-sec. Heretofore it has been assumed that the primary mechanism for the recombination of atomic ions was by means of radiative recombination, for which Bates and Massey[2] had calculated a rate constant of $\alpha = 10^{-12}$ cm^3/ion-sec. In searching for a more efficient process, Bates[3] suggested that recombination in the noble gases occurs through the neutralization of molecular ions, with the subsequent dissociation of the unstable molecule. This process is known as dissociative recombination.

In dissociative recombination, recombination is seen as occurring in two stages. Thermal electrons are captured by molecular ions forming the complex $[AA^+ + e]$. As a result of a radiationless transfer, an excited molecule AA^*, is formed from the complex. If this resultant molecule is in a repulsive state, its constituent atoms may move apart. After the atoms have increased their separation beyond a certain critical distance, the electron can no longer detach itself from the ion. From a rough quantum mechanical calculation of a rate constant for dissociative recombination, Bates obtained the value of $\alpha = 10^{-7}$ cm^3/ion-sec. Bates' formulation shows that dissociative recombination can be sufficiently rapid to account for the experimentally observed rates. The temperature variation predicted for dissociative recombination from this analysis is $T^{-3/2}$.

The hypothesis of dissociative recombination has proved to be extremely fruitful to the study of afterglow in plasmas. The presence of molecular ions in helium, neon, argon, and mercury plasmas at pressures where recombination is appreciable (above 1 mm Hg pressure) has been verified. At the lower pressures, where diffusion is the dominant process, atomic ions are the significant ionic species present. In order to demonstrate conclusively the dependence of gas phase recombination on the presence of molecular ions, Biondi[4] studied the behavior of small concentrations of argon in helium and neon. The experimental conditions were such that only the argon was ionized but the concentration of argon was too low to permit appreciable formation of Ar_2^+. Under these conditions, electron decay followed a rate law characteristic of ambiopolar diffusion rather than recombination.

The publication in 1957 of Persson's paper[5] on the limitations of conventional microwave cavity methods inaugurated an intensive re-evaluation of experimental data. Prior to Persson's study, the linearity of a plot of $1/n$ vs t was assumed to constitute proof of gas phase recombination. More rigorous analysis indicates that the decay of diffusion-controlled plasma may follow a linear $1/n$ vs t rate law because of the presence of higher order diffusion modes. Gray and Kerr have established stricter criteria for the interpretation of microwave results by obtaining an exact numerical solution of the partial differential equation governing the decay of electron density in an afterglow. They find that a linear plot is conclusive only if in the interval of observation the electron density varies by at least a factor of five.[7]

The analysis of Gray and Kerr provides insight into some recent results for noble gas plasmas. Oskam[8] has studied the electron loss in helium, neon, and argon, extending his observations to the later afterglow. He confirmed the presence of He_2^+ and Ne_2^+ in their respective plasmas and $NeHe^+$ ions in helium-neon mixtures. Ne_2^+ and He_2^+ were observed to undergo dissociative recombination, in agreement with Biondi; however, the primary loss mechanism for He_2^+ appeared to be by ambipolar diffusion even at pressures as high as 25 mm Hg. On analyzing the original data of Biondi and Brown, Gray and Kerr[7] note that for neon and argon the linear regions are very extensive, with the electron density varying by a factor of 15 for neon and 50 for argon. In the case of helium, the $1/n$ vs t plot remains linear only over a factor of 3 or 4 in electron density.

At present, then, the mechanism of dissociative recombination is considered to be firmly established in the case of neon and argon; the behavior of helium is still uncertain. Spectroscopic evidence[9,10,11] indicates that in the <u>early</u> afterglow He_2^+ ions are present in highly excited vibrational states; these species participate in dissociative recombination. In later periods of the helium afterglow, beyond 2 milliseconds,

He_2^+ persists in the plasma, but in a form which resists recombination. This change in the reactivity of the He_2^+ is attributed to vibrational de-excitation in the later afterglow. The loss in ionization is then largely by ambipolar diffusion of He_2^+ and electrons. In the region where diffusion predominates, Kerr[7] estimates an upper limit of $\alpha = 2 \times 10^{-9}$ cm^3/ion-sec for recombination.

2. Diatomic Gases

The decay of plasmas derived from diatomic gases exhibits distinct differences from the monatomic gases. The investigation by Persson and Brown[12] of hydrogen plasmas is of particular significance. They found that in very pure hydrogen, when higher modes of diffusion are properly accounted for, ion-electron recombination does not occur. This finding contradicts the earlier results of Biondi and Brown,[13] and Varnerin.[14] It is now presumed the kinetics in the earlier studies was distorted by trace impurities; specifically, moisture and oxygen. In the absence of impurities, the ionized species are removed by ambipolar diffusion.

The question of the identity of the primary positive ion in hydrogen plasmas produced at room temperatures is only now being resolved. It had been assumed that the form of the positive ion was H_2^+. However, on the basis of a study of secondary reactions occurring in the ion source of mass spectrometers, Stevenson[15] concluded that H_3^+ is formed,

$$H_2^+ + H_2 \rightarrow H_3^+ + H \quad , \tag{25}$$

with a very large cross section for formation, $\sigma = 10^{-14}$cm^2. Stevenson assigns a binding energy of 4.18 ev to H_3^+. Varney[16] interprets Stevenson's results as implying that indeed H_2^+ is never observed at room temperatures, but, rather H_3^+ is the primary ion, and H_3^+ possesses the properties usually attributed to H_2^+.

The behavior of nitrogen plasmas at room temperatures has been studied by Faire.[17, 18] The basic microwave techniques were supplemented by a monochromator and photomultipliers in order to analyze the radiation emitted in the afterglow. The decay of electron density was attributed to a combination of gas phase recombination and ambipolar diffusion. The value of the diffusion coefficient was used to correct the apparent value of the recombination rate constant for electron losses due to fundamental mode diffusion. The magnitude of higher mode diffusion losses was estimated and found to be small. The corrected value of the rate constant is

$$\alpha = 4.0 \times 10^{-7} \text{ cm}^3/\text{ion-sec} \quad . \tag{26}$$

The spectroscopic analysis disclosed that the radiation is dominated by emission arising from the nitrogen second positive band system. Occasionally, N_2^+ bands are also observed. The evidence from optical spectroscopy indicates that in nitrogen plasmas at room temperatures the molecular species predominate.

The recombination process is attributed by Faire to dissociative recombination

$$N_2^+ + e \rightarrow N + N \quad . \tag{27}$$

No direct experimental justification for this choice of mechanism is presented beyond fitting the data to a second order rate law.

The decay of nitrogen plasmas at elevated electron temperatures has been investigated by Sayers.[19, 20] In his experimental arrangement the plasma is studied in a discharge tube. The ionization is produced by radio frequency discharges between electrodes placed within the tube. Electron temperatures and electron densities are determined with a

Langmuir wire probe. Simultaneously, changes in ion densities are measured with a miniature radio frequency mass spectrometer (similar to the mass spectrometer probe described previously). The rate of disappearance of N_2^+ ions was found to follow a second order rate law. The recombination coefficients at electron temperatures of 2000° and 3200° K are 5×10^{-7} cm^3/ion-sec and 1.1×10^{-7} cm^3/ion-sec.

Comparison of Sayers' values with the value of 4×10^{-7} cm^3/ion-sec obtained by Faire for thermal electrons suggests that the ionic constituents in the two experiments may be different. Along this line, some results from ion drift velocity studies in nitrogen merit consideration. By means of mass spectroscopic analyses, Varney[21, 22] has identified N_4^+ as primary ion in the gas at low temperatures and field strengths (E/p_o below 60 volts/cm mm Hg). At higher temperatures and field strengths N_2^+ predominates. The ion ratio at room temperature and an E/p_o of 70 is estimated to be one-to-one. In view of these observations, the incorporation of mass spectroscopic analyses into microwave discharge experiments is clearly necessary.

In oxygen plasmas at room temperatures and pressures in the range of 1-100 mm Hg, the primary mechanism of electron loss is by attachment to oxygen molecules. The details of the process were long unclear and are only now being resolved. Electron attachment studies in a drift tube, by Bradbury[23], yield an apparent attachment cross section of $10^{-19} cm^2$, but microwave afterglow experiments by Biondi[24] and Holt[25] gave cross sections of $10^{-22} cm^2$. One significant difference in the conditions of the two types of experiment is that the lowest electron energies in drift tubes were ~0.2 ev, while the microwave studies where carried out at thermal energies, 300°K = 0.04 ev. The development of a modified drift tube[26] permitted the study of attachment down to 0.03 ev, resulting in a clarification of the phenomena involved.

The recent drift tube results confirm that at low electron energies attachment is a third order process,

$$\frac{dn_e}{dt} = - k (O_2)^2 n_e \tag{28}$$

and generally lend support to the scheme devised by Bloch and Bradbury[27] to explain Bradbury's original data. By this scheme, low energy attachment occurs by a two-step process: Acquisition of an electron by an oxygen molecule occurs with the formation of a short-lived, vibrationally excited negative ion. This excited ion reverts back to the initial state of a neutral molecule and a free electron unless it undergoes a stabilizing collision to remove its excitation energy. Specifically,

$$O_2 + e \rightleftarrows (O_2^-)_{\nu=1} \tag{29}$$

$$(O_2^-)_{\nu=1} + (O_2)_{\nu=0} \rightarrow (O_2^-)_{\nu=0} + (O_2)_{\nu=1} \tag{30}$$

where ν = 0, 1 refer to the ground and first vibrational states, respectively. The transfer process may involve a transfer of vibrational energy or a transfer of the electron. The experimental data reveals the presence of a threshold at $\sim$0.1 ev, such as would be required to excite the first vibrational state of the negative ion. Some preliminary evidence obtained by Schulz[28] indicates that at somewhat higher electron energies the molecular ion is excited to the higher vibrational levels, ν = 2, 3, etc. The experimental work also indicates that the third order attachment reaction does not go over to a second order reaction at $\sim$5 mm Hg, as assumed by Bloch and Bradbury; no deviation from third order kinetics for pressures in excess of 50 mm is seen in the data.

At electron energies above 3.5 ev, a different process, dissociative attachment, becomes operative:

$$O_2 + e \rightarrow O^- + O \quad . \tag{31}$$

This reaction exhibits second order kinetics and has been studied in the drift tube[26] and the data compared to the results obtained in electron beam experiments.[29] The agreement in the data from the two techniques is quite good, confirming the belief that dissociative attachment may contribute significantly to the loss of electrons whenever electron energies become appreciable.[30]

At considerably lower oxygen pressures, in the range of 10^{-3} to 10^{-2} mm Hg, the dominant electron loss process is observed to be recombination rather than attachment. In experiments in discharge tubes with a Langmuir probe and time-of-flight mass spectrometer, Sayers[20, 21] found that at an oxygen partial pressure of 0.015 mm, O_2^+ was the primary ion present in the afterglow and its decay obeyed second-order kinetics. (Sufficient helium was added to the system to suppress diffusion; the total pressure was 0.34 mm.) The values determined for the recombination coefficient are 6×10^{-8} cm^3/ion-sec at an electron temperature of 2000°K and 4×10^{-8} cm^3/ion-sec at 2500°K.

When the oxygen partial pressure is reduced still further, the proportion of O^+ ions in the plasma increases; at a partial pressure of 0.005 mm oxygen O^+ is the main species at the beginning of the afterglow. In the presence of excess oxygen molecules, O^+ is removed from the system by a first order rate law,

$$\frac{d(O^+)}{dt} = k(O^+) \quad . \tag{32}$$

A similar result is found in kinetic studies of the ionosphere, for which Bates evolved the mechanism of ion-atom interchange

$$O^+ + O_2 \rightarrow O_2^+ + O \tag{33}$$

followed by O_2^+ - electron recombination

$$O_2^+ + e \rightarrow O + O \quad . \tag{34}$$

The arguments advanced by Bates in support of the above mechanism are reviewed under Ionization Processes in the Atmosphere.

Sayers[31] recently published the results of his evaluation of the rate constant for oxygen interchange reaction. He employed the same experimental setup containing a discharge tube and mass spectrometer and helium was added to the system to suppress diffusion. Rate measurements were made at four temperatures, 204°, 263°, 276°, and 300°K. The resulting rate constants are 2.6×10^{-11}, 2.2×10^{-11}, 2.4×10^{-11} and 3.0×10^{-11} cm^3/ion-sec, respectively.

A study of electron loss processes in nitric oxide plasmas has been reported recently.[32] The plasma was produced by photoionization by Lyman α radiation. The plasma was found to consist of NO^+ ions, electrons and neutral NO molecules. The decay of ionization was followed in an X-band microwave cavity. The primary mechanism of electron disappearance was by attachment to NO molecules by a three-body, Bloch-Bradbury process. The attachment rate coefficient measured is 5×10^{-31} cm^6/particles-sec at an electron energy of about 0.1ev. Under the experimental conditions, electron attachment proved to be an effective competitor to ion-electron recombination.

3. Metallic Vapors

The mechanism of electron density decay in the plasmas of metallic vapors has also been investigated. The behavior of mercury plasmas produced by microwave discharge at elevated temperatures was studied by Dandurand and Holt.[33] and Biondi.[34] Cesium plasmas in arc discharges were studied by Mohler[35] and in microwave discharges by Dandurand and Holt.[36] In each case the data from the two sources are contradictory and a detailed examination of experimental procedures is required before a choice between the results can be made.

In the case of mercury it is possible to choose between the conflicting results. Holt's work has been criticized by Loeb[37] as lacking in a meticulous regard for the experimental difficulties that arise in microwave research. In particular, it was suggested that the short microwave excitation times (10 μsec) and short observation times (less than 100 μsec) were inadequate to ensure that the plasma was fully established. Biondi's study was made in helium-mercury mixtures in order to reduce diffusion losses and provide that the electrons possessed only thermal energy. Biondi finds that, while Hg^+ is formed by the discharge, recombination occurs through the formation of the molecular ion, Hg_2^+:

$$Hg^+ + 2Hg \rightarrow Hg_2^+ + Hg \quad . \tag{35}$$

The Hg_2^+ then reacts with electrons by dissociative recombination:

$$Hg_2^+ + e \rightarrow Hg^* + Hg \quad . \tag{36}$$

Biondi's value for the recombination rate constant is $\alpha = 5.5 \times 10^{-7}$ cm^3/ion-sec (at 400°K); Holt's is $\alpha = 5 \times 10^{-9}$.

The case of cesium is more complicated and a definitive study has yet to be made. Mohler studied cesium plasmas in an arc discharge. The electron temperature was sestimated to be 1200°K. Mohler obtained a value of 3.6×10^{-10} cm^3/ion-sec for the recombination rate constant from photometric measurements, and 3.4×10^{-10} cm^3/ion-sec from ionization probes. Dandurand and Holt used microwave techniques and obtain fairly linear plots of the inverse of electron density with time, indicating recombination. Their spectroscopic observations revealed that the afterglow radiation is a molecular band spectrum. Holt proposes that recombination occurs with the formation of Cs_2^+, which combines with an electron to give highly excited states of Cs_2. The band spectrum is attributed to the de-excitation of the Cs_2 molecule. Loeb[38], on the other hand, feels that it is more likely that Cs_2^+ recombines dissociately with electrons and he attributes the band spectrum to subsequent reaction of the excited atoms to form metastable Cs_2^* species.

The values obtained from the electron-ion recombination measurements are shown in Table 1.

B. Shock Wave Ionization

The basic phenomena observed in shock tubes arise from processes which re-establish thermodynamic equilibrium in the shock-heated gas. The fundamental observational quantity is the relaxation time, the time that elapses between the arrival of the shock front and the attainment of equilibrium. The relaxation time represents a result of all the rate processes by which the gas may distribute the excessive transitional energy acquired from the shock wave. The first reactions in the gas immediately after the passage of the shock wave are endothermic processes. However, as thermodynamic equilibrium is approached, reverse exothermic reactions become increasingly effective and, at equilibrium, endothermic and exothermic processes are precisely counterbalanced. In studying ionization mechanisms with shock tubes, therefore, it must

Table 1

Electron-Ion Recombination Measurements

Gas	Electron Temperature °K	Pressure mmHg	Electron Density electrons/cm^3	Recommened Coefficient cm^3/ion-sec	Comments	Reference
Helium	300°	< 3	$\sim 10^{11}$		ambipolar diffusion of He^+ and e	Kerr[7]
	300°	> 3	$\sim 10^{11}$	2×10^{-9}	dissociative recombination: He_2^++e; ambipolar diffusion of He_2^+ predominates	Kerr[7] Oskam[8]
Neon	300°	5-30	10^{10}-10^{11}	2.07×10^{-7}	dissociative recombination: Ne_2^++e	Biondi, Brown[13]
	300°	4-20	5×10^8-5×10^{10}	1.1×10^{-7}	dissociative recombination: Ne_2^++e	Oskam[8]
Argon	300°	20-30	10^{11}	8.8×10^{-7}	dissociative recombination: Ar_2^+e	Biondi[4]
Helium-Neon Mixtures	300°	5-23	5×10^8-5×10^{10}	4.3×10^{-7}	dissociative recombination $(HeNe)^+$+e (0.5-1.3% neon)	Oskam[8]
Hydrogen	300°	3-60	$\sim 10^{10}$	$< 3 \times 10^{-8}$	ambipolar diffusion of H_3^+ and e is the dominate process	Persson and Brown[12]
Nitrogen	300°	0.01-4	10^9	4.0×10^{-7}	possibly dissociative recombination. Identity of the specific ion uncertain	Faire and Champion[18]
	2000°	$\sim$0.08	10^{10}	5.0×10^{-7}	dissociative recombination: N_2^++e (discharge tube)	Sayers[20]
	3200°	0.015	$\sim 10^{10}$	1.1×10^{-7}	dissociative recombination (discharge tube; He added, total pressure ~ .3mm)	Sayers[19]
Oxygen	300°	5-50			molecular attachment of electrons by a three-body process $K = 2.8 \times 10^{-30} cm^6/particles^2$ -sec at thermal energies (drift tube)	Chain, Phelps & Biondi[26]
	200-300°	0.002-0.025	$\sim 10^{10}$		ion-atom interchange: $O^+ + O_2 \rightarrow O_2^+ + O$. $K = 2.5 \times 10^{-11} cm^3$/ion-sec over the temperature range. (Discharge tube; He added, total press. ~ 1 mm)	Dickinson & Sayers[31]
	2000°	$\sim$0.08	10^{10}	6×10^{-8}	dissociative recombination: O_2^++e (discharge tube)	Sayers[20]
	2500°	0.015	$\sim 10^{10}$	4×10^{-8}	dissociative recombination: O_2^++e (discharge tube; He added, total pressure 0.35 mm)	Sayers[19]
Nitric Oxide	300°	> 10	10^9-10^{10}		molecular attachment of electrons by a three-body process. $K = 5 \times 10^{-31} cm^6/particles^2$ sec	Gunton & Inn[32]
Mercury	400°	1.4-1.6	10^9-10^{10}	5.5×10^{-7}	dissociative recombination: Hg_2^++e	Biondi[34]
Cesium	1200°	0.01-0.1	1.8×10^{12}	3.6×10^{-10}	probably dissociative recombination (arc)	Mohler[35]

Unless otherwise noted, the measurements were made in microwave cavities be remembered that the observed ionization relaxation times represent the resultant of opposing reactions, ionization and neutralization. Hence, the relaxation time, per se, is an ambiguous parameter and cannot be used as the sole criterion for distinguishing between ionization mechanisms. Rather it is necessary to follow the course of the reaction by the continuous measurement of the fundamental properties of the system such as the electron density. Simultaneously the critical intermediates in the ionization reactions must be detected and their concentrations determined as a function of time.

1. Exploratory Experiments

The first shock tube studies which were reported were of an exploratory nature. The primary interest of the investigators was in the fluid dynamic aspects of shocks and in confirming the aerodynamic and thermodynamic theories of the equilibrium conditions behind strong shocks. The gaseous systems which received the greatest attention were air and argon: air, because it is the only gas considered to be of importance by earthbound aerodynamicists; argon, because in it one avoids the complications of molecular dissociation. Over the years as experience was gained and technology advanced these two gaseous systems have been investigated with increasing sophistication.

The most extensive investigation of the ionization of gases by means of shock tubes is the program of Kantrowitz and his colleagues, and by Lin. Their first report[39] set forth the relevant fluid dynamic and thermodynamic calculations used for the production of strong shocks. The preliminary experimental results showed that the observed shock strengths were in good agreement with theoretical calculations. On the basis of the shock strengths measured, it was calculated that temperatures as high as 18000°K were attained in argon. A highly luminous region was found to be associated with the shock front in argon and air. At that time it was not possible to obtain spectrographs of the shock front;

exposure times were too short for the spectrographic equipment then available. The first efforts to measure the electrical conductivity of the plasma by probes and magnetic induction were not too successful, and the investigators were convinced that conductivity in a highly ionized gas is a complicated phenomenon.

The refinement of experimental techniques permitted fuller investigation of radiation and electrical conductivity in argon plasmas.[40,41] Spectrograms of the shock front revealed a strong continuum which accounted for most of the observed luminosity. The prominent argon lines in the spectrum were broadened and shifted toward the longer wavelengths. The wavelength shifts were up to 4Å. The drum camera spectrograms revealed that the shift reached a maximum very quickly after the onset of luminosity. By interpreting the line broadening and shift as due to a Stark effect produced by random electric fields of the high ion densities in the plasma, the line shift was used to determine the ion density utilizing the theoretical treatment of this problem by Baranger.[42,43] The measurements based on the Baranger theory indicated that the shock-heated argon reaches ionization equilibrium well within the testing times available with shock tubes. These findings demonstrated the general feasibility of shock tubes for the study of ionization kinetics.

In their study of electrical conductivity in argon plasmas Kantrowitz's group encountered some of the same difficulties with probes which were encountered by experimenters in gaseous electronics. The conductivity measured by the probes was as much as a thousand times smaller than theoretical calculations. Furthermore the measured conductivity did not show the anticipated dependence on initial densities. These discrepancies were attributed to boundary layer effects. In order to avoid the surface effects inherent in probe measurements, the electrical conductivity was determined by magnetic induction, utilizing the interaction between a magnetic field and the moving plasma. The maximum conductivity measured thereby agreed within 10 percent of calculations based on the Spitzer-Harm theory of conductivity in highly ionized gases. The magnetic induction technique has proved to be very useful in the study of ionization in air where the visible spectrum is dominated by molecular band radiation, reducing the effectiveness of spectroscopy.

2. Rare Gases

The accumulated experience with ionization in shock tubes enabled Petschek and Byron[44] to investigate the ionization kinetics of argon. In this work the rate of change of electron density was determined by electrostatic probes and continuum intensity measurements. Oscillograms were obtained of the potential of a single probe relative to a grounded resistance wire running parallel to the shock tube. The resistance wire provided a reference potential at a point fixed in a coordinate system moving with the shock wave. The oscillograph traces exhibit a sharp jump at the passage of the shock wave. This is followed by a flat region; at low electron densities the probe voltage is apparently independent of electron density. As the electron density increases the signal rises with increasing slope. Finally the probe voltage becomes constant indicating that equilibrium has been achieved. An expression derived for the sheath potential, ϕ, of the probe in the region of high electron densities relates the change in probe potential with distance behind the shock wave, x, to the electron densities,

$$\frac{e}{kT_e}\frac{d\phi}{dx} \approx \frac{d(\ln n_e)}{dx}. \qquad (37)$$

The general shape of the oscillograms is in agreement with this relation.

The continuum radiation emitted by an ionized gas arises from the recombination of ions and electrons. The intensity of the radiation is proportional to the number of electron-ion collisions or the square of the electron density. Therefore, the time variation of the electron density during the approach of equilibrium may be obtained by measuring the intensity of the continuum radiation with a photomultiplier. The shape of the oscillograms of the continuum intensity profile is in qualitative agreement with potential measurements described above. The signal rises from essentially zero with increasing slope and finally flattens off to a constant value.

The general shape of the oscillograms obtained from light intensity and probe potential measurements agrees with a rate law derived from the assumption that the ionization is produced by electron-atom collisions. For a more quantitative comparison, the measured values of the maximum rate of change of potential were plotted on a curve calculated from the rate law and the expected probe response. The agreement is fairly good, although the experimental points tend to run high. Comparison of the measured logarithmic derivative of the continuum intensity at one-fourth the equilibrium intensity with the calculated derivative based on the theoretical rate law indicates somewhat better agreement. The agreement improves with increasing enthalpy, perhaps due to the fact the rate becomes less sensitive to the value of the inelastic cross section at high enthalpy. The experimental results are, therefore, consistent with the mechanism of ionization occurring by electron-atom impacts. However, the mechanism of atom-atom collisions for the onset of ionization does not seem to be operative under the conditions of the experiments. The drum camera spectrograms provide data on the time required by the shock-heated argon to reach ionization equilibrium. The logarithm of the relaxation time is found to depend almost linearly on the reciprocal of the initial atom temperature. On the other hand, at a given temperature the relaxation time is independent of the density. If ionization were initiated by atom-atom collisions, the relaxation time would be inversely proportional to the initial argon pressure. But if the initial ionization were catalyzed by the presence of impurities in the argon, then the relaxation time would be independent of pressure because the impurity level n_i/n_{Ar} varies with the initial argon pressure.

A study of the kinetics of ionization in xenon has been reported recently by Johnston and Kornegay.[43] Since the experiment raises a number of significant theoretical and technical questions, it will be described in detail. The rate of ionization was measured behind reflected shock waves in a shock tube that was made from rectangular waveguide. The reaction rate was determined from the absorption by free electrons of microwaves propagated longitudinally down the shock tube. The ionization kinetics was determined over the temperature range of 3400-7600°K for pure xenon, and xenon-neon mixtures. The cardinal objective of the experiments was to obtain an accurate estimate of the activation energy for xenon ionization.

In order to obtain an accurate value of the activation energy for xenon ionization, the chief parameter varied in the experiments was the temperature. Initial conditions were adjusted to attain reactant pressures in the vicinity of 2.6 atm in the pure xenon runs and 1.2 atm in the 17.8%Xe-82.2%Ne mixtures. The electron densities were in the 5×10^{10} - 5×10^{11} range. In the reflected shock zone a constant rate of ionization was observed after a time interval of the order of 10μsec. A plot of the logarithm of the values of the constant rate R against $1/kT$ gave an activation energy of about 8 ev for both pure xenon and the xenon-neon mixtures.

The experimentally determined value of about 8 ev for the activation energy is significantly less than the ionization potential of 12.13 ev for xeon, but lies close to the values of the lower excited electronic states: ^3P at 8.3 ev, ^1P at 8.4 ev, ^1D at 9.6 ev and ^3S, ^3P, ^3D at 9.4 ev. Johnston and Kornegay reason, therefore, that xenon ionization proceeds through the formation of electronically excited intermediates, collectively denoted as Xe*:

$$Xe + M \underset{k_2}{\overset{k_1}{\rightleftarrows}} Xe^* + M$$

$$Xe^* + M \xrightarrow{k_3} Xe^+ + e + M \qquad (38)$$

where M represents a third body molecule.

The corresponding differential rate equations are

$$\frac{dn_e}{dt} = k_3(Xe^*)(M) \tag{39}$$

$$\frac{d(Xe^*)}{dt} = k_1(Xe)(M) - (k_2 + k_3)(Xe^*)(M) \tag{40}$$

The fact that the degree of ionization in the experiments is 10^{-5} or less and, therefore, the xenon concentration is essentially constant, permits a direct solution of the rate equations. Solving Eq. (40) for the concentration of excited xenon, Xe*:

$$\frac{(Xe^*)}{(Xe)} = \frac{k_1}{k_2 + k_3}\left[1\text{-}\exp\text{-}(k_2 + k_3)(M)t\right] \tag{41}$$

the rate of electron production is

$$R(t) = \frac{dn_e}{dt} = \frac{k_1 k_3}{k_2 + k_3}\,(Xe)(M)\left[1\text{-}\exp\text{-}(k_2 + k_3)(M)t\right] \tag{42}$$

or

$$R(t) = R_{ss}\left[1\text{-}\exp\,(\text{-}Bt)\right] \tag{43}$$

where R_{ss} is the steady state rate, $R_{ss} = (k_1k_3/k_2 + k_3)\,(Xe)(M)$, and $B = (k_2 + k_3)(M)$.

This generalized formulation must be applied to the conditions in the shock tube in order to extract the values of the individual rate constants. At each point along the tube the gas is in a different stage of the reaction. At a given point z behind the reflected shock wave the gas has been ionizing for a time τ,

$$\tau(z) = t - z/C_s \tag{44}$$

where C_s is the shock velocity and t is the time at the onset of the reflected shock. The microwave absorptivity is a function of the total number of electrons $(e)_T$ in the shock tube, and the derived rate law Eq. (42) must be expressed in terms of this quantity:

$$\frac{d(e)_T}{dt} = A\int_0^z R(z)dz = AC_s\int_0^t R_{ss}\,[\,1-\exp\,(-Bt)]\;dt \tag{45}$$

A is the cross sectional area of the shock tube. Therefore,

$$\frac{d(e)_T}{dt} = AC_s\, R_{ss}t\,[\,1 - 1/Bt\,(1-\exp - Bt)] \tag{46}$$

and

$$(e)_T = (\tfrac{1}{2}\, AC_s\, R_{ss}t^2)\, f \tag{47}$$

where

$$f = 1 - \frac{2}{Bt} + \frac{2}{B^2t^2}\,[\,1-\exp\,(-Bt)]$$

An approximate value for f is obtained by expanding the exponential and retaining the first term, $f_o = Bt/3$.

The microwave absorptivity is given by

$$D = \log I_o/I = \beta_o n_e z = \beta_o(e)_T/A \quad . \tag{48}$$

Therefore, the ionization rate is determined from the change in the absorptivity:

$$R = R_{ss}f(t) = \frac{2}{\beta_o C_s} \frac{\left(\sqrt{D_2} - \sqrt{D_1}\right)^2}{(t_2 - t_1)^2} \tag{49}$$

R_{ss} is determined directly from the flat portion of the ionization rate curve; B from the initial slope of a plot of R/R_{ss} vs t.

The empirical rate factors were assumed by Johnston and Kornegay to have the following identities:

$$R_{ss} = k_a(Xe)(M) \tag{50}$$

$$B = k_b(M) \quad . \tag{51}$$

The activation energies E_a were determined from the steady state rates R_{ss} by plots of log k_a vs $1/T$. Similarly, the values of E_b were determined from B. The results are given in the following table:

System	E_a (ev)	E_b (ev)
Xe	7.4 ± 1.1	3.9 ± 2.3
Xe - Ne	7.7 ± 0.7	3.3 ± 0.8

Johnston and Kornegay note that the values of E_a may be taken to be 8.4 ev within experimental error, and accordingly assign the value of 8.4 to E_a. The value of the activation energy is taken as confirmation of the mechanism:

$$Xe + M \underset{k_2}{\overset{k_1}{\rightleftharpoons}} Xe^* + M \tag{52}$$

$$Xe^* + M \rightarrow Xe^+ + e + M \quad . \tag{53}$$

On the basis of this mechanism,

$$R_{ss} = k_a(Xe)(M) = \frac{k_1 k_3}{k_2 + k_3}(Xe)(M) \tag{54}$$

$$B = k_b(M) = (k_2 + k_3)(M) \quad . \tag{55}$$

The activation energy of 8.4 is associated with the formation of the electronically excited species Xe^*. Therefore, the rate of formation of Xe^* is the rate determining step in the ionization of xenon. In consequence of this interpretation, the Xe^* never attains its equilibrium concentration and $k_3 >> k_2$. That is,

$$k_a = k_1 \quad \text{and} \quad k_b = k_2 \quad ,$$

the result which is obtained when k_2 is neglected with respect to k_3 in Eq. (54) and (55).

In a critical study of the Johnston-Kornegay paper, Alpher and White[46] tested the implications of the mechanism with the experimental data. The mechanism requires that the equilibrium concentration of Xe^* is never attained and that $k_3 >> k_2$. Therefore,

$$\frac{k_1}{k_3} << \frac{k_1}{k_2} < \left(\frac{Xe^*}{Xe}\right)_{eq} \quad . \qquad (56)$$

Alpher and White compare the ratio of the empirical rate constants ($k_1 = k_a$ and $k_3 = k_b$) with the equilibrium concentration ratio $(Xe^*/Xe)_{eq}$, taking $E_a = 8.4$ ev. as shown in Table 2.

Table 2

Comparison of Rate Constant Ratios with Equilibrium Concentration Ratios

	T	k_1/k_2	$(Xe^*/Xe)_{eq} = g^*/g_o \exp(-E_a/kT)$
xenon	5324	3.2×10^{-8}	$g^*/g_o \times 1.9 \times 10^{-8}$
	5850	3.6×10^{-8}	$g^*/g_o \times 5.6 \times 10^{-8}$
	6525	4.9×10^{-8}	$g^*/g_o \times 3.4 \times 10^{-7}$
	7525	1.4×10^{-7}	$g^*/g_o \times 2.4 \times 10^{-6}$
xenon neon mixture	4250	1.6×10^{-7}	$g^*/g_o \times 1.0 \times 10^{-10}$
	5325	3.3×10^{-7}	$g^*/g_o \times 1.9 \times 10^{-8}$
	6100	4.4×10^{-6}	$g^*/g_o \times 1.1 \times 10^{-7}$
	7565	1.2×10^{-5}	$g^*/g_o \times 9.1 \times 10^{-4}$

The intermediate Xe^* must therefore encompass a large number of electronically excited states in order for the factor g^*/g_o to be large enough to satisfy the inequality of Eq. (56)

Alpher and White also point out that on the basis of the rate data presented, it is not possible to make a unique determination of the activation energy. Depending on the nature of the temperature dependence assumed, one obtains the following values of the activation energy. For pure xenon,

Rate law	Activation energy
$k \propto T^{1/2} e^{-E/kt}$	7.08 ± 0.58
$k \propto e^{-E/kT}$	7.34 ± 0.58
$k \propto T^{-1/2} e^{-E/kT}$	7.60 ± 0.58

It is clear that care must be taken in applying an Arrhenius type of analysis to kinetic data that covers a 3200° temperature range.

The most puzzling aspect of the experimental results is that no matter which temperature dependence is adopted, the empirical activation energy is less than the lowest excited state of xenon. To assume that E_a is really 8.4 ev and blame any discrepancy on experimental error is to beg the question. Since the microwaves are transmitted longitudinally down the shock tube, they provide an integrated result of all ionizing processes occurring in the tube. It is possible that the rate data would be more meaningful if various secondary process are accounted for. For example, as the expansion wave propagates through the low pressure gas region, a rarefraction wave is transmitted through the high pressure region and is reflected from the back face of the shock tube. Photoemission from the walls of the tube may also enhance the ionization. In view of the inadequacy of the mechanism involving an activation energy of 8.4 ev, a deeper insight into the fluid dynamics and the ionization processes of the experiment is required for the interpretation of the experimental results.

3. Atomic Hydrogen

The rate of recombination of electrons with atomic hydrogen ions was measured by Fowler and Atkinson[47] by observing the expanding plasma in an electrically energized shock tube.[48] The determination was based on measurements of the absolu e intensity in the continuum associated with the Balmer spectrum and of the positive ion concentration. The ion concentration was estimated from the Stark broadening of the Balmer line H_β by using a modification of Holtzmark's theory.[49] The values for the recombination coefficient derived by assuming that all the photons are produced by recombination lie between 1×10^{-12} and 2×10^{-12} cm^3/ion-sec for $n_e = 10^{16}/cm^3$ and $Te \approx 4500°K$. There is evidence, however, that some of the continuum beyond the Balmer series is due to the affinity spectrum of hydrogen produced by electron attachment. The rate constant agrees roughly with those calculated by Cillie,[50] $\alpha = 7 \times 10^{-13}$ to 1×10^{-12} cm^3/ion-sec, and disagrees with experimental results of Olsen and Huxford,[51] whose measurements were not made in a field-free region.

4. Air

In a continuing experimental program, Lin is studying the ionization of air in shock tubes. An earlier study[52] of the electrical conductivity of shock-heated air indicated that the ionization process builds up very quickly behind the shock front. The conductivity was determined by the magnetic induction technique described previously and the measured conductivity at equilibrium agreed satisfactorily with theory. In recent studies the rate of ionization is measured by microwave reflection as well as by magnetic induction. The first experiments were performed in 1-1/2 inch diameter shock tubes similar to the one used in the conductivity studies. However, the ionization of air proved to be too fast to be clearly resolved under these conditions. In order to get adequate rate data Lin resorted first the study of oxygen-nitrogen mixtures containing as little as 1/4 percent oxygen so as to slow down the electron production rate.[53] Finally, Lin constructed a 24-inch diameter shock tube, which permitted him to operate at considerably lower initial air densities.[54]

The most recent experimental results[55] again indicate that the rate of ionization in air is extremely fast, several orders of magnitude faster than that in argon at corresponding shock strengths. The maximum electron density gradient appears to be proportional to the second power of the initial pressure, suggesting that the dominant processes leading to ionization involve binary collisions. According to Lin, the mechanisms developed for the ionization of argon are inappropriate for air, and he attributes the very fast electron production rate in air to inelastic, atom-atom collisions of the type

$$N + O \rightarrow NO^+ + e, \quad E_o^o = 2.8 \text{ ev}$$
$$N + N \rightarrow N_2^+ + e, \quad E_o^o = 5.8 \text{ ev}$$
$$O + O \rightarrow O_2^+ + e, \quad E_o^o = 6.9 \text{ ev}$$

This hypothesis is strengthened by the absence of a long induction period for air ionization and the mild shock-velocity dependence of the ionization rate. An extensive analysis of the experimental results by Lin and Teare has been promised, but it has not yet appeared. We are told, however, that inclusion of the three ionization reactions given above into the AVCO shock tube performance calculations yields self-consistent results.

C. Photoionization Cross Sections

1. Monatomic Gases and Metallic Vapors

The mechanisms of absorption in the rare gases and the alkali metal vapors are the least complicated, and the spectra are easily interpreted in terms of the removal of a single electron from the atom. This interpretation is verified by the fact that values of photoionization and photoabsorption cross sections coincide.

In argon,[56] photoabsorption begins at the first ionization limits at 786.72 and 777.96Å, which correspond to the $^2P^o_{3/2}$ and $^2P^o_{1/2}$ states of the argon ion. A region of pre-ionization lies between the two ionic states. The absorption lines from electronic transitions of the atom which fall in this region are broadened because of the adjacent $^2P^o_{3/2}$ continuum and the probability of radiationless transitions into it. A second peak in the photoabsorption curve occurs at 424Å and arises from the removal of a 3s electron from the argon atom, yielding the $^2S_{1/2}$ state of the ion. Between the $^2P^o_{1/2}$ and $^2S_{1/2}$ edges a number of absorption points lie above the curve. These may be assumed to result from pre-ionization converging on $^2S_{1/2}$.

Entirely analogous features are observed in the absorption spectrum of neon,[57] with the difference that the region of pre-ionization between the doublet ground states of the ion is only 2Å wide. On the other hand, helium shows no pre-ionization.[58] The photoionization cross sections for helium, neon, and argon are shown in Figure 7.

The absorption curves for the alkali metals have several interesting features in common.[59] As the series limit is approached from the long-wave side, the number of absorption lines in a given small-frequency region increases. The width of the lines increases and the absorption becomes truly continuous on the long-wave side of the limit. There is a sharp peak in the absorption at the series limit. Photoionization starts on the long-wave side of the limit and has been studied in detail by Mohler[60] in the case of cesium. He accounts for the pre-ionization in terms of collisions between photo-excited and normal atoms to form molecular ions. On the short-wave side beyond the series limit absorption reaches a pronounced minimum and then increases. Early theoretical studies indicated that there should be no minimum. However, Bates[61] showed that when the polarization

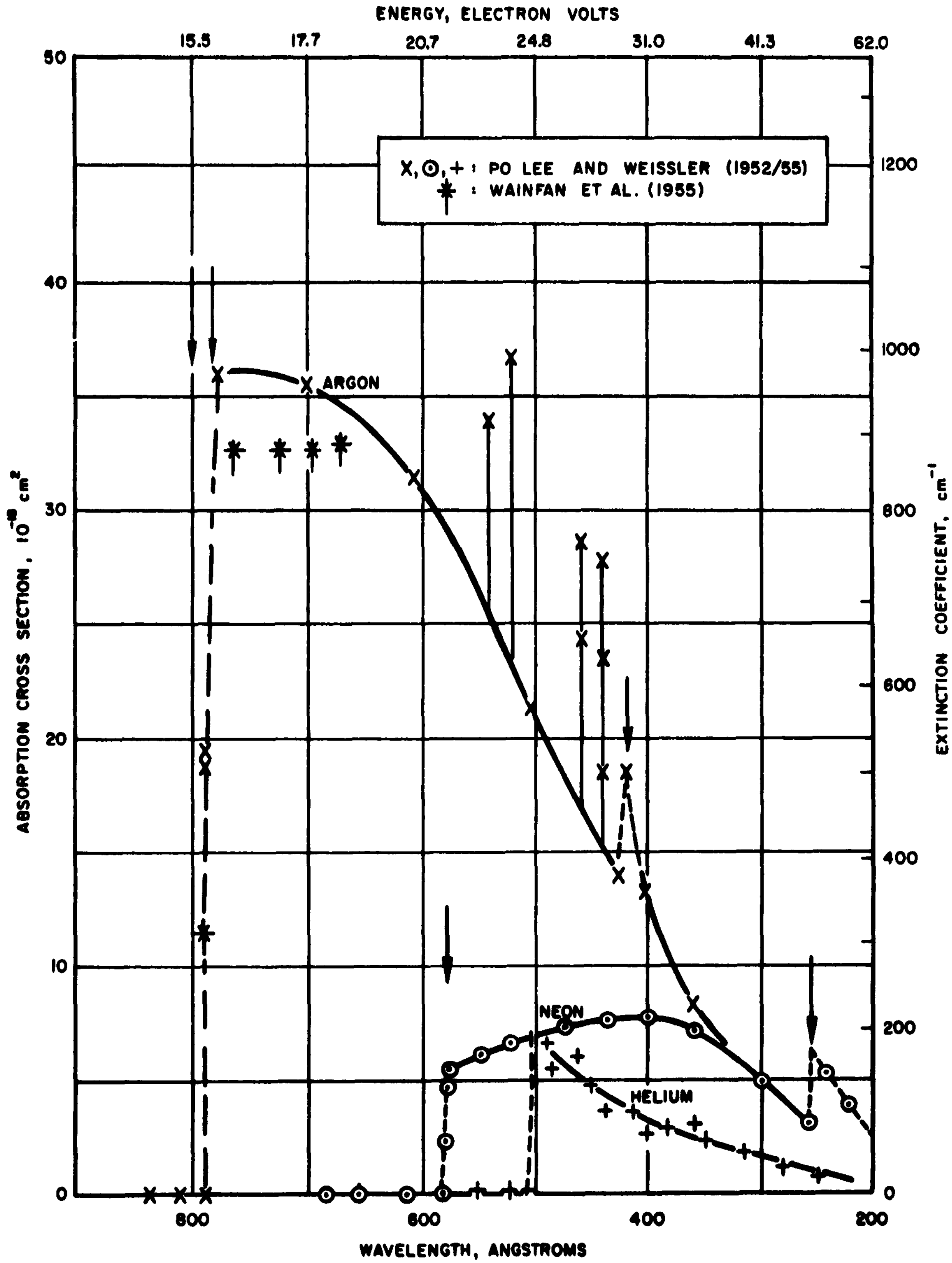

Figure 7. Photoionization in Helium, Neon and Argon

of the atomic core was taken into account, a minimum was obtained. Refined calculations by Seaton[62] for sodium, in which the finite minimum in the absorption is attributed to spin-orbit perturbations of the free electron wave functions, reproduce the main features of the experimental curve. The photoionization cross sections for sodium and potassium are shown in Figures 8 and 9.

2. Molecular Gases

The photoabsorption spectra of the molecular gases are considerably more complicated and their interpretation more tentative. For example, in the case of oxygen three continuous regions can be distinguished. Immediately adjacent to the Schumann-Runge bands the dissociation continuum starts at 1750Å, obtains a maximum at 1450Å and extends to 1300Å.[63] The second continuum appears at the first ionization limit at 1040Å and reaches a maximum at 910Å. The absorption decreases until about 850Å, where it is overlapped by a new region of strong continuous absorption. Between 850Å and 740Å there are many closely spaced, diffuse bands. Beyond 740Å a smooth absorption contour is obtained, representative of the main ionization continuum, with a maximum at 510Å.[64] In this region, bands are observed with higher absorption coefficients than the continuum.[65] These bands indicate the presence of pre-ionization in oxygen. The bands have been grouped into Rydberg series progressions converging to four distinct series limits. The main continuum below 763Å may be interpreted as a superposition of three ionization processes.[66,67]

The absorption spectrum of nitrogen is less complex. The intense resonance bands observed between 600 and 1000Å have been analyzed into Rydberg series which converge on two limits at 796Å and 661Å.[68,69] Therefore, the continuum that arises below 800Å may be attributed to a photoionization process. This interpretation is substantiated by Wainfan's[65] direct measurements of photoionization which are in

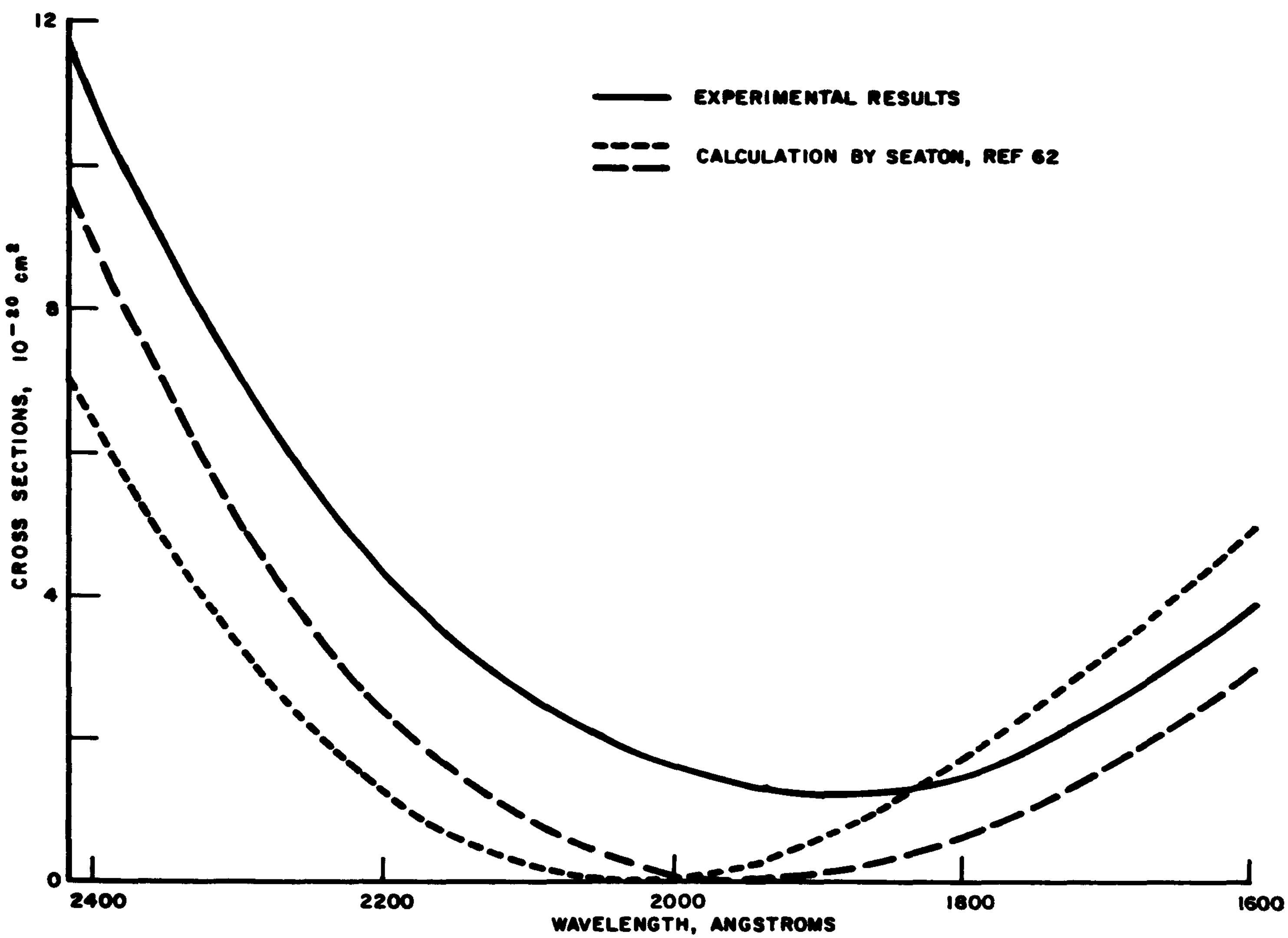

Figure 8. Photoionization in Sodium Vapor, Beginning at the Series Limit, 2410Å

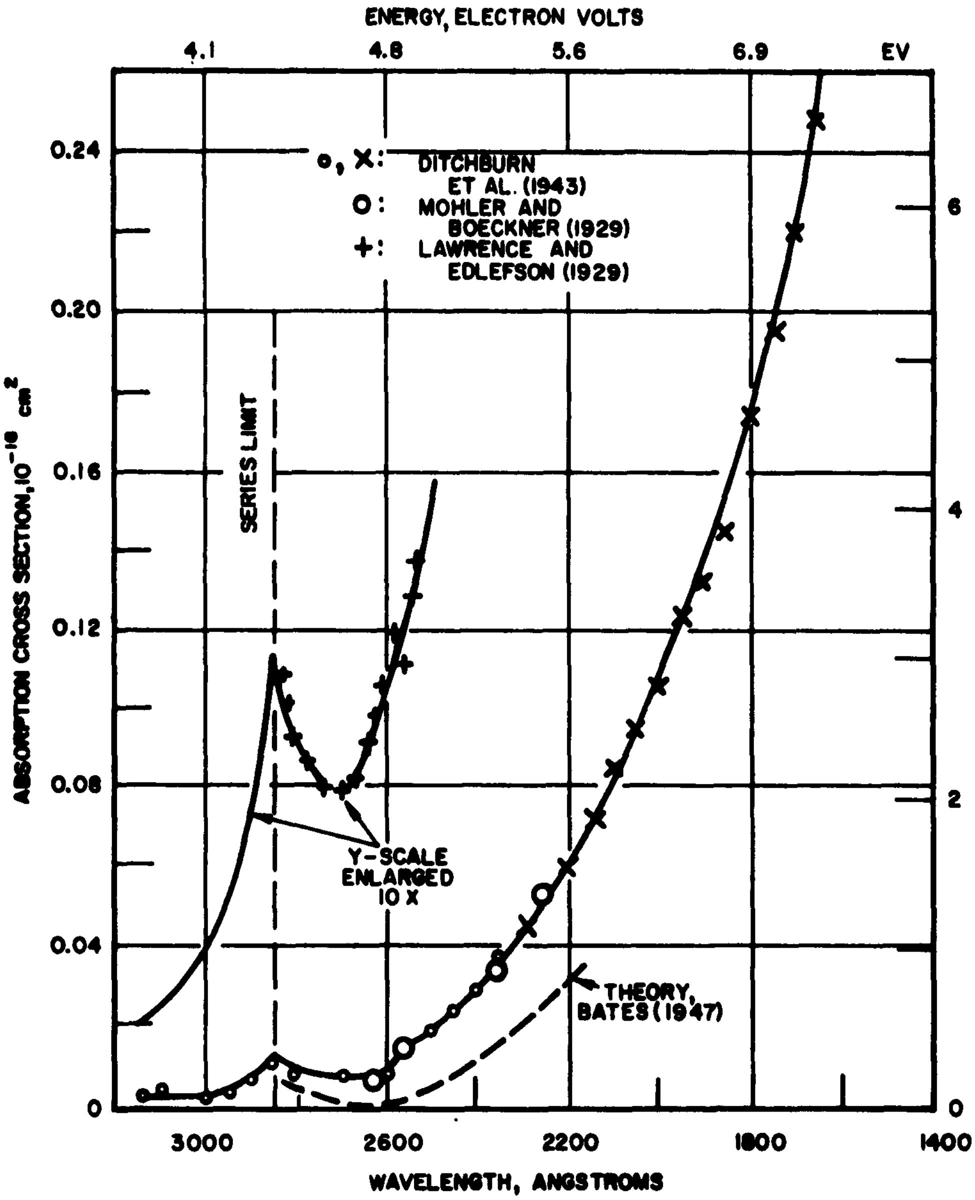

Figure 9. Photoionization in Potassium Vapor

agreement with the photoabsorption contour.[70] The direct measurements also indicate an absence of pre-ionized bands in nitrogen.

In the absorption spectrum of nitric oxide weak bands are found between 1350 and 1600Å. The onset of photoionization occurs at 1343Å.[70] Two additional maxima occur in the absorption curve, at 920Å and 620Å. The preliminary photoionization data of Walker and Weissler[72] are not spaced sufficiently close to enable these investigators to decide whether the peaks are due to a dissociation or an ionization process. The dissociative ionization reaction

$$NO \rightarrow N^{+} + O^{-*}$$

occurs in the vicinity of 620Å[73] and it is possible that the peak is due to this process superimposed on the ionization continuum.

The data on photoionization in molecular hydrogen is not sufficiently complete to permit a definitive analysis. Both sharp and diffuse bands together with a dissociation continuum are observed between 770 and 850Å. Because of their overlapping with the ionization limit at 803.7Å it has proved difficult to identify the ionization continuum.[74] The photoionization absorption of hydrogen is shown in Figure 10.

The absolute photoionization cross sections of polyatomic molecules described above, determined with a vacuum monochromator combined with an ion collector, represent the <u>total</u> cross sections of the ions produced at a given wavelength without regard to specific identity of the ions that are formed. In gases where molecular dissociation is possible, more than one species of ions may be formed. For example, in oxygen, both O_2^+ and O^+ are produced below 658Å, but the fraction of the total cross section due to the formation of O_2^+ and the fraction due to O^+ is not revealed by the measurement. Using a windowless monochromator - mass spectrometer

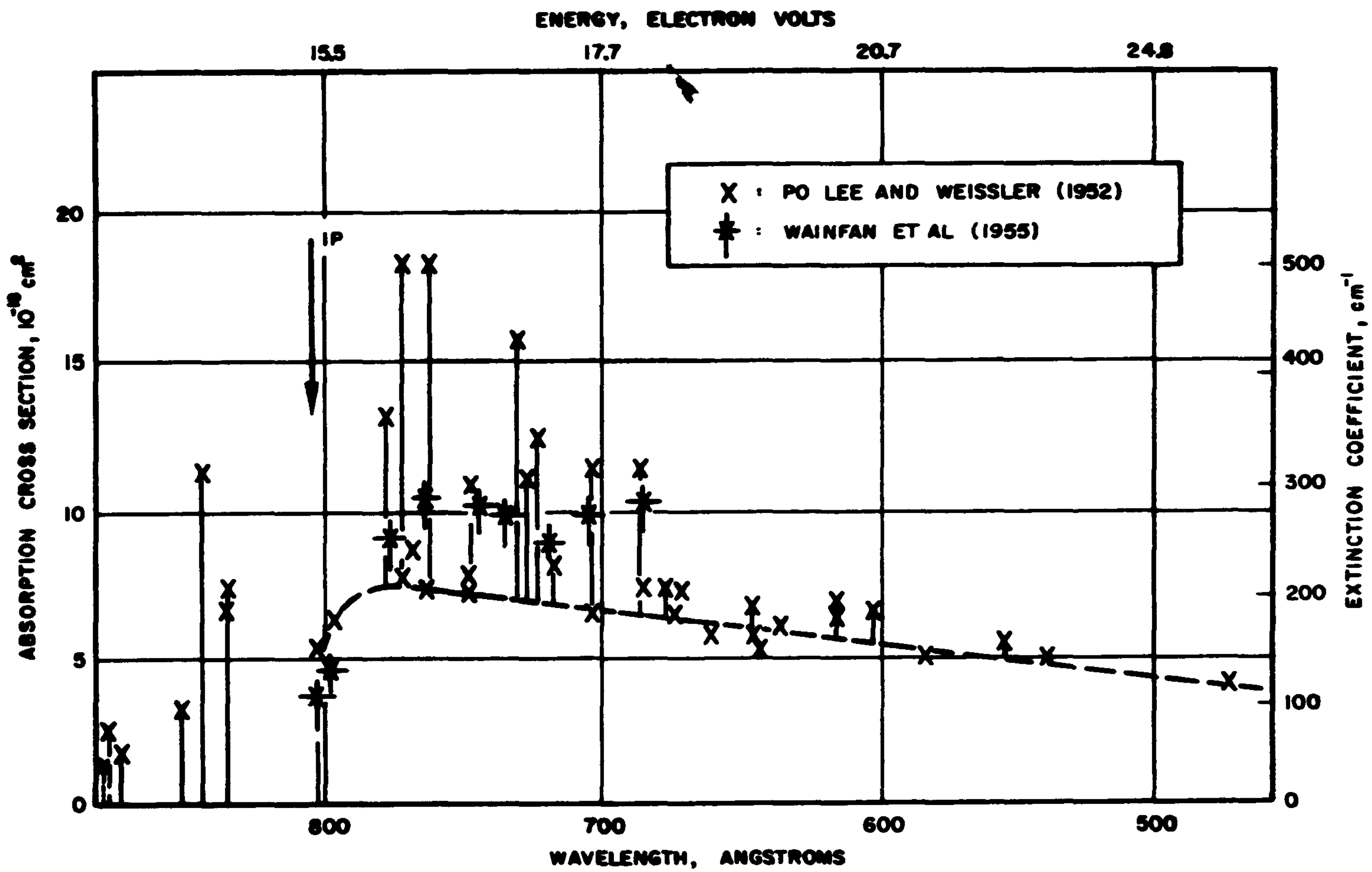

Figure 10. Photoionization of Hydrogen

combination Weissler and his associates have determined the relative yields of the various ion fragments produced from molecular ions.

The results from Weissler's[75] study show that, with the exception of N_2O and NO_2, dissociative processes yielding atomic ions account for only 1 to 10 percent of the ions formed. A comparison of the atomic and molecular ion intensity versus wavelength curves helps to elucidate the features observed in the total absorption curves described above. By interpreting the initial rise of each absorption peak as the photon impact appearance potential of the ion in the next higher excited state, the photoionization results can be correlated with electron impact and spectroscopic data. In the absorption spectra of oxygen, shown in Figure 11, the photon impact appearance potentials are indicated by the arrows. Many peaks are observed in both the O_2^+ and O^+ curves and the associated electronic states are identified in Table 3. The determination of appearance potentials of O_2^+ from the initial rise of the O_2^+ peaks agrees closely with the values measured by spectroscopy. This agreement supports the contention that the absorption peaks are due to the formation of O_2^+ in states of higher electronic excitation. The appearance potential at 14.3 ev may, however, be due to pre-ionization.

In the O^+ curve, two peaks are resolved and a third peak partially resolved. The initial rise of the first two peaks occurs at 18.8 ev (658Å) peak is about 23.4 ± 0.5 ev (530 ± 12Å).

An examination of the potential energy curves, applying the Frank-Condon principle, suggests that the O^+ at 658Å is formed from the dissociation of the O_2^+ $(A^2\Pi_u)$ state into O^+ (^4S) and O (^3P). The additional O formed at 598Å may be attributed to the dissociation of the $b^4\Sigma_g^-$ state into O^+ (^4S) and O^* (^1D); however, it is likely that at this energy the dissociation process is $O_2 \rightarrow O^{+*}$ (^2D) + O^- (^2P) since O^- has been observed in this region in the electron impact experiments.[76]

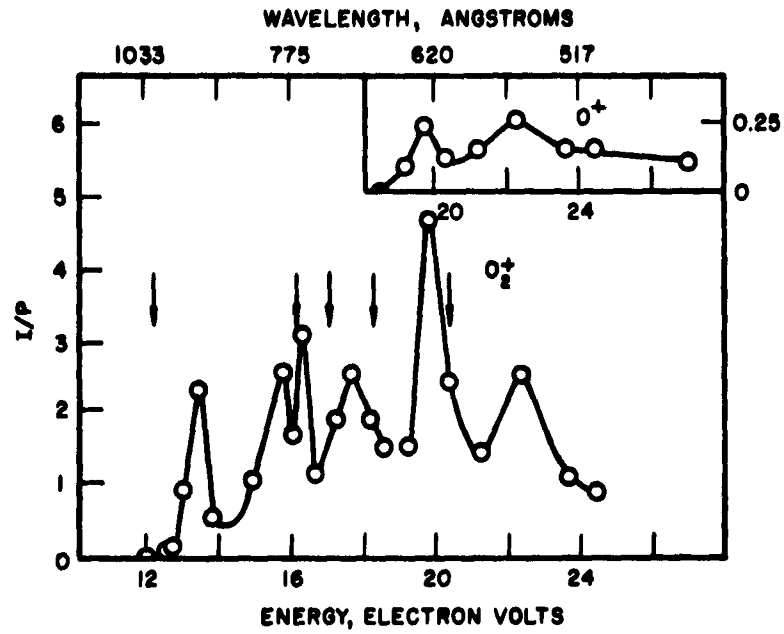

Figure 11. O_2^+ and O^+ Yields from the Photoionization of Oxygen. The Arrows Indicate the First and Higher Ionization Limits

Table 3

Appearance Potentials of O_2^+

Electronic State	Photon Impact Appearance Potential	Spectroscopic Ionization Potential
$X\,^2\Pi_g$	12.2 ev	12.15 ev
$a\,^4\Pi_u$	15.9	16.1
$A\,^2\Pi_u$	16.9	17.0
$b\,^2\Sigma_g^-$	18.8	18.2
	21.2	20.3

In the absorption spectra for nitrogen shown in Figure 12, the photon impact appearance potentials are indicated by the arrows. The values for the appearance potentials for N_2^+ are shown in Table 4. The determination of the ionization potential of N_2 from the ionization curve agrees with the spectroscopic values. The N^+ ion appears at 24.3 ±0.2 ev (510 ±5Å). The N^+ ion arises from the dissociative ionization of N_2: $N_2\ (X\ ^1\Sigma_g^+) \rightarrow N^+\ (^3P) + N\ (^4S)$.

In the absorption spectra for nitric oxide shown in Figure 13, the photon impact appearance potentials are indicated. The values for the appearance potentials for NO^+ are shown in Table 5. In the case of NO the derived appearance potentials agree with the three series limits found by Tanaka and a $A\ ^1\Pi$ state. The unidentified appearance potentials near the α series limit may be related to pre-ionization since diffuse bands have been observed in this region. Dissociative ionization processes contribute little to the total photoionization cross section of NO, at least above 400A. Atomic oxygen and nitrogen ions are formed, but their relative abundance are only of the order of 2 percent for O^+ and 5 percent for N^+ at 21.8 ev (the energy at the maximum N^+ abundance). The formation of N^+ may be attributed to the process, $NO\ (X^2\Pi) \rightarrow N^+(^3P) + O\ (^3P)$; the O^+ ion intensities were too small to identify the ionization process.

The photoionization cross sections are presented in Table 6.

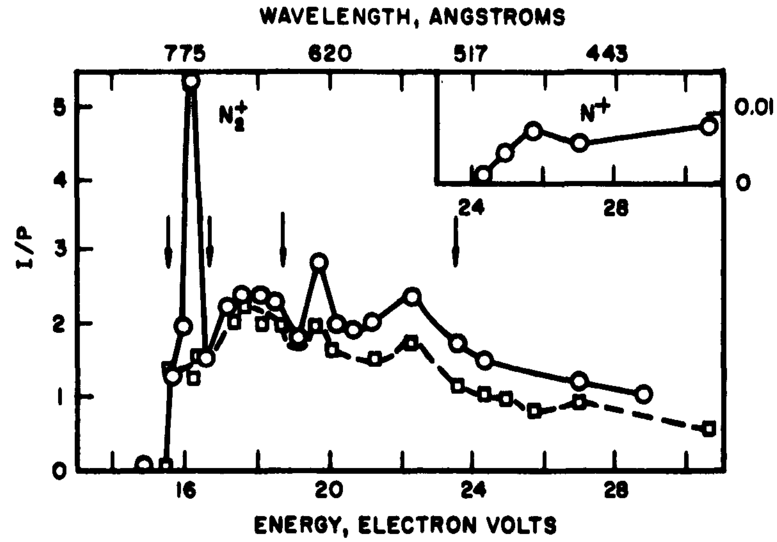

Figure 12. The N_2^+ and N^+ Yields from the Photoionization of Nitrogen

Table 4

Appearance Potentials of N_2^+

Electronic State	Photon Impact Appearance Potential	Spectroscopic Ionization Potential
$X\ {}^2\Sigma_g^-$	15.6	15.576
$A\ {}^2\Pi_u$	16.9	16.71
$B\ {}^2\Sigma_u^+$	18.8	18.748
$C\ {}^2\Sigma_u^+$	--	23.581

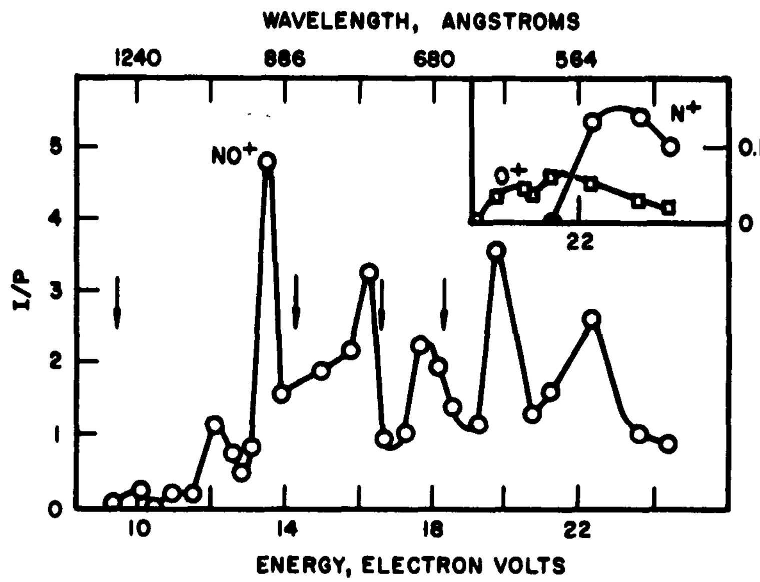

Figure 13. The NO^+, O^+ and N^+ Yields from the Photoionization of Nitric Oxide

Table 5

Appearance Potentials of NO^+

Electronic State	Photon Impact Appearance Potential	Spectroscopic Ionization Potential
$X\,^1\Sigma^+$	9.2	9.25
a	14.2	14.23
β	16.9	16.56
γ, $A\,^+\Pi$	18.8	18.32, 18.36

Table 6

Photoionization Cross Sections of Gases and Metallic Vapors

Monatomic Gas	Gases and Vapors Ionization Potential	Cross Section at Ionization Limit ($\times 10^{-18}$ cm^2)	Reference
Helium	24.58 ev, 504.27Å	7.3	PoLee and Weissler[58]
Neon	21.56 ev, 574.94Å	5.5	PoLee and Weissler[57]
Argon	15.75 ev, 786.72Å	35	Wainfan et. al.[56]
Lithium	5.39 ev, 2300Å	2.5	Tunstead[77]
Sodium	5.14 ev, 2410Å	0.116	Ditchburn et. al.[59]
Potassium	4.34 ev, 2860Å	0.12	Ditchburn et. al.[78]
Rhubidium	4.18 ev, 2972Å	0.11	Mohler and Boeckner[60]
Cesium	3.89 ev, 3185Å	0.23	Mohler and Boeckner[60]
Magnesium	7.61 ev, 1629Å	1.2	Ditchburn and Marr[79]
Calcium	6.09 ev, 2036Å	0.45	Jutsum[80]
Indium	5.76 ev, 2153Å	0.3	Marr[81]
Thallium	6.07 ev, 2043Å	4.5	Marr[82]

Table 6

Photoionization Cross Sections of Gases and Metallic Vapors (continued)

Molecular Gases Molecular Ions	Ionization Potential	Max. Photoionization Cross Section ($\times 10^{-18}$ cm^2)	Reference
Hydrogen	15.42 ev, 804Å	9.3 (750Å)	Wainfan et. al.[56]
Nitrogen	15.58 ev, 796Å	26.3 (750Å)	Wainfan et. al.[56]
Oxygen	12.15 ev, 1020Å	27.9 (600Å)	Wainfan et. al.[56]
Carbon Dioxide	13.73 ev, 903Å	34.6 (650Å)	Wainfan et. al.[56]
Water	13.0 ev, 955Å	20.1 (600Å)	Wainfan et. al.[56]
Atomic Ions			
Nitrogen	15.6 ev, 795Å	0.2 (480Å)	Weissler et. al.[75]
Oxygen	18.8 ev, 658Å	1.7 (645Å)	Weissler et. al.[75]

REFERENCES

1. M.A. Biondi and S.C. Brown, Phys. Rev. 75, 1700 (1949).

2. D.R. Bates, R.A. Buckingham, H.S.W. Massey and J.J. Unwin, Proc. Roy Soc. A170, 322 (1939).

3. D.R. Bates, Phys. Rev. 77, 718 (1950), 78, 492 (1950).

4. M.A. Biondi, Phys. Rev. 83, 1078 (1951); 90, 730 (1953).

5. K.B. Persson, Phys. Rev. 106, 191 (1957).

6. E.P. Gray and D.E. Kerr, 12th Annual Gaseous Electronics Conference, Washington, D.C., Oct. 1959, abstract in Bul. Amer. Phys. Soc. 5, 122 (1960).

7. E.P. Gray and D.E. Kerr, Proc. 4th Internat'l Conf. on Ionization Phenomena in Gases, Page 84, North-Holland Publishing Co., Amsterdam (1960).

8. H.J. Oskam, Philips Res. Rept 13, 335, 401, (1958).

9. M.A. Biondi and T. Holstein, Phys. Rev. 82, 962 (1951).

10. D.E. Kerr and C.S. Leffel Jr, 11th Annual Gaseous Electronics Conference, New York, Oct. 1958; abstract in Bul. Amer. Phys. Soc. 4, 113 (1959).

11. W.A. Rogers and M.A. Biondi, Phys. Rev. to be published

    M.A. Biondi, "Atomic Collision Processes involving Electrons and Ions in Atmospheric Gases", Advance Papers of an International Symposium on Chemical Reactions in the Lower and Upper Atmosphere, Stanford Research Institute, (1961).

12. K.B. Persson and S.C. Brown, Phys. Rev. 100, 729 (1955).

13. M.A. Biondi and S.C. Brown, Phys. Rev. 76, 1697 (1949).

14. L.J. Varnerin, Phys. Rev. 84, 563 (1951).

15. D.P. Stevenson and D.O. Schissler, J. Chem. Phys. 29, 282 (1958).

16. R.N. Varney, Phys. Rev. Letters 5, 559 (1960).

17. A.C. Faire, O.T. Fundingsland, A.L. Aden, K.S.W. Champion, J. Appl. Phys. 29, 928 (1958).

18. A.C. Faire and K.S.W. Champion, Phys. Rev. 113, 1 (1959).

19. J. Sayers, "Recent Laboratory Studies in Recombination Cross-sections" in Solar Eclipses and the Ionosphere, (suppl. to Vol. 6 Atmosph. Terr. Phys.), 212, Pergmon Press, London, 1956.

20. J. Sayers and L.W. Kerr, 3rd International Conference on Ionization Phenomena in Gases, p. 908, Rendiconti, Milan, 1957.

21. F.R. Kovar, E.C. Beaty and R.N. Varney, Phys. Rev. 107, 1490 (1957).

22. R.N. Varney, "Molecular Ions," Proceedings of the 4th International Conference on Ionization Phenomena in Gases, P. 69, North-Holland Publishing Co., Amsterdam, 1960.

23. N.E. Bradbury, Phys. Rev. 44, 883 (1933).

24. M.A. Biondi, Phys. Rev. 84, 1072A (1951).

25. E. Holt, Bul. Amer. Phys. Soc. 4, 112 (1959).

26. L.M. Chanin, A.V. Phelps and M.A. Biondi, Phys. Rev. Letters 2, 344 (1959).

27. F. Block and N.E. Bradbury, Phys. Rev. 48, 689 (1935).

28. G.J. Schulz, paper C-5 13th Annual Gaseous Electronics Conference, Monterey, Oct. (1960).

29. J.D. Craggs, R. Thorburn and B.A. Tozer, Proc. Roy Soc. A240, 473 (1957).

30. M.A. Biondi, "Measurements of Electron Attachment, Recombination, Elastic and Inelastic Collisions in the Atmospheric Gases," Physical Chemistry in Aerodynamics and Space Flight, page 104, Pergamon Press, New York (1961). Reprinted in Planet Space Sci. 3, 104 (1961).

31. P.H.G. Dickinson and J. Sayers, Proc. Phys. Soc. (Lond.) 76, 137 (1960).

32. R.C. Gunton and E.C.Y. Inn, paper C-6, 13th Annual Gaseous Electronics Conference, Monterey, (Oct. 1960).

33. P. Dandurand and R.B. Holt, Phys. Rev. 82, 868 (1951).

34. M.A. Biondi, Phys. Rev. 90, 730 (1953).

35. F.L. Mohler and C. Boeckner, J. Res, Nat. Bur. Stand 2 (1929); C. Boeckner, J. Res, Nat. Bur. Stand 6, 277 (1931); F.L. Mohler, J. Res. Nat. Bur. Stand 10, 771 (1933), 19, 447, 559 (1937).

36. P. Dandurand and R.B. Holt, Phys. Rev. 82, 278 (1951).

37. L.B. Loeb, Basic Processes of Gaseous Electronics, p. 583, 2nd revised ed, Univ. of California Press, Berkeley (1960).

38. L.B. Loeb, ibid page 591.

39. E.L. Resler, S.C. Lin and A.R. Kantowitz, J. Appl. Phys. 23, 1390 (1952).

40. H.E. Petschek, P.H. Rose, H.S. Glick, A Kane, A. Kantrowitz, J. Appl. Phys. 26, 83 (1955).

41. S.C. Lin, E.L. Resler and A. Kantrowitz, J. Appl. Phys. 26, 95 (1955).

42. M. Baranger, Phys. Rev. 111, 494 (1958).

43. Advances in the theory of Stark broadening are discussed in papers by H.R. Griem and A.C. Kolb, and by H. Margenom, 4th International Conference on Ionization Phenomena in Gases North-Holland Publishing Co., Amsterdam (1960).

44. H. Petschek and S. Byron, Ann. Phys. (N.Y.) 1, 270 (1957).

45. H.S. Johnston and W. Kornegay, Trans. Fara. Soc., to be published.

46. R.A. Alpher and D.R. White, private communication.

47. R.G. Fowler and W.R. Atkinson, Phys. Rev. 113, 1268 (1959).

48. R.G. Fowler, W.R. Atkinson, W.D. Compton and R.J. Lee, Phys. Rev. 88, 137 (1952).

49. H. Hoffman and O. Theimer, Astrophys. J. 127, 477 (1958).

50. G. Cillie, Mon. Notices, Roy. Astron. Soc, 92, 820 (1931/32).

51. H. Olsen and W. Huxford, Phys. Rev. 87, 927 (1952).

52. L. Lamb and S. C. Lin, J. Appl. Phys. 28, 754 (1957).

53. S. C. Lin, Avco-Everett Research Laboratory Res. Rept. 33, (June, 1958).

54. S. C. Lin, Avco-Everett Research Laboratory Res. Note 170 (Dec. 1959).

55. S. C. Lin, R. A. Neal and W. I. Fyfe, Avco-Everett Research Laboratory Res. Rept. 105 (Sept. 1960).

56. PoLee and G. L. Weissler, Phys. Rev. 99, 540 (1955), N. Wainfran, W. C. Walker, and G. L. Weissler, Phys. Rev. 99, 542 (1955).

57. PoLee and G. L. Weissler, Proc. Roy. Soc. A219, 71 (1953).

58. PoLee and G. L. Weissler, Phys. Rev. 99, 540 (1955).

59. A review of the experimental work in the alkali vapors is given in R. W. Ditchburn, P. J. Jutsum and G. U. Marr, Proc. Roy. Soc, A219 89 (1953).

60. F. L. Mohler and C. Boeckner, J. Res. Nat. Bur Stand 3, 303 (1929).

61. D. R. Bates, Proc. Roy Soc. A188, 350 (1947).

62. M. J. Seaton, Proc. Roy Soc. A208, 418 (1951).

63. R. W. Ditchburn and D. W. O. Heddle, Proc. Roy Soc. A220, 61 (1953).

64. G. L. Weissler and PoLee, J. Opt. Soc. Amer. 42, 200 (1952). PoLee, J. Opt. Soc. Amer. 45, 730 (1955).

65. N. Wainfan, W. C. Walker, and G. L. Weissler, J. Appl. Phys. 24, 1318 (1953); Phys. Rev. 99, 542 (1955).

66. W.C. Price and G. Collins, Phys. Rev. 48, 714 (1935).

67. Y. Tanaka, J. Chem. Phys. 20, 1728 (1952).

68. R.E. Worley, Phys. Rev. 64, 207 (1943).

69. Y. Tanaka and T. Takamine, Sci. Pap. Inst. Phys. Chem. Res., Tokyo 39, 427 (1942).

70. G.L. Weissler, PoLee and E.I. Mohr, J. Opt. Soc. Amer. 42, 84 (1952).

71. K. Watanabe, J. Chem. Phys. 22, 1564 (1954).

72. W.C. Walker and G.L. Weissler, J. Chem. Phys. 23, 1962 (1955).

73. H.D. Hagstrum, Rev. Mod. Phys. 23, 185 (1951).

74. PoLee and Weissler, Astrophys. J 115, 570 (1952) also, N. Wainfan et.al. Phys. Rev. 99, 542 (1955).

75. G.L. Weissler, J.A.R. Samson, M. Ogawa and G.R. Cook, J. Opt. Soc, Amer. 49, 338 (1959).

76. H.D. Hagstrum, J. Chem. Phys. 23, 1178 (1955).

77. J. Tunstead, Proc. Phys. Soc. (London) A66, 304 (1953).

78. R.W. Ditchburn, J. Tunstead, and J.G. Yates, Proc. Roy Soc. A181, 386 (1943).

79. R.W. Ditchburn and G.V. Marr, Proc. Phys. Soc. (London) A66, 655 (1953).

80. P.J. Jutsum, Proc. Phys. Soc. (London) A67, 196 (1954).

81. G.V. Marr, Proc. Phys. Soc. (London) A67, 196 (1954).

82. G.V. Marr, Proc. Roy Soc. A224, 83 (1954).

SECTION V

IONIZATION PROCESSES IN THE ATMOSPHERE

In the high atmosphere of the earth there exist distinct layers of ionization. The most distinct of these are the E and F regions; at night these are located at altitudes near 100 and 150 km, respectively. During the day, as a result of the photoionizing effect of solar radiation, the F region bifurcates, with the F_1 layer near 180 km and the F_2 layer at 250 km and above. Below the E region lies a less well defined region of ionization known as the D layer; it is normally only weakly ionized, but its ionization is considerably enhanced during periods of solar activity.

The presence of the ionosphere was first revealed by the behavior of radio waves in the atmosphere. Heaviside and Kennelly postulated the existence of a conducting layer order to account for long distance radio transmission, discovered by Marconi. The properties of this layer were deduced from radio reflectance experiments. The height of the layer was determined by triangulation, and the electron density from the frequency of the radio signal:

$$n_e = m_e \omega^2 / e^2 \quad . \tag{57}$$

(m_e and e are the mass and charge of the electron, respectively.) The experimental results (E. V. Appleton) indicated that the reflecting layer was at a height of 80-90 km and had an electron density of 2 x 10^5 per cm^3. This is the E layer. Later it was discovered that, as the frequency of the radio signals is increased beyond a certain critical frequency ω_c between 4 and 5 mc/sec, the reflectance disappears and at higher frequencies reappears. These results show that there is a maximum electron density in the E layer, so that frequencies greater than ω_c cannot be reflected by this region; they are reflected, then, at a considerably greater height from a region of greater electron density. In this manner the F layer was revealed. If the signal frequency is further increased above 9 mc/sec, the reflectance again disappears, indicating a maximum electron density in the F layer of 6×10^5 per cm^3. In daytime, critical frequencies corresponding to two levels of maximum ionization are observed; these levels are termed the F_1 and F_2 layers. The presence of the D layer was inferred by Appleton from the familiar experience that the reception of distant radio stations improves markedly soon after dusk. The D layer lies below the E layer at about 80 km during the daytime and disappears entirely at night. The electron density estimated from absorption measurements is about 3×10^2 per cm^3.

Some of the difficulties inherent in the ground based radio experiments, such as the effect of the E layer on signals reflected from the F layer, are overcome by the use of rockets. A signal transmitted from the ground and received by a rocket passes through the ionized region only once and need not satisfy any condition of reflection. One type of measurement involves transmitting two pulses, one of very high frequency which suffers no retardation, the other slightly above the critical frequency, which is appreciably retarded as it crosses the ionized layers. The difference in their time of arrival is a measure of the electron density of the layer traversed. The rocket experiments have shown that the layers are lower than estimated from ground radio results.

A summary of our present knowledge of the ionosphere is presented in Tables 7 and 8. The total particle density is derived from an analysis of satellite drag.[1] The altitude distributions of the neutral constituents were calculated by Bates[2] based on the consideration that diffusion is the

Table 7

Properties of the Ionosphere

Altitude (km)	Temp. (°K)	Number Density (particles/cm^3)			Mass (gm/cm^3) Density
		O	O_2	N_2	
120	380	1.8×10^{11}	4.0×10^{10}	2.4×10^{11}	1.8×10^{-11}
160	938	2.6×10^{10}	2.0×10^{10}	1.6×10^{10}	2.5×10^{-12}
200	1031	1.1×10^{10}	4.4×10^{8}	4.1×10^{9}	5.0×10^{-13}
250	1048	4.9×10^{9}	7.9×10^{7}	9.2×10^{8}	1.8×10^{-13}
300	1050	2.1×10^{9}	1.5×10^{7}	2.2×10^{8}	6.7×10^{-14}
350	1050	9.4×10^{8}	3.0×10^{6}	5.2×10^{7}	2.7×10^{-14}
400	1050	4.2×10^{8}	6.0×10^{5}	1.3×10^{7}	1.2×10^{-14}
450	1050	1.9×10^{8}	1.6×10^{5}	3.2×10^{6}	5.2×10^{-15}
500	1050	8.8×10^{7}	2.6×10^{4}	8.2×10^{5}	2.3×10^{-15}
600	1050	1.9×10^{7}	1.2×10^{3}	5.7×10^{4}	5.1×10^{-16}
700	1050	4.4×10^{6}	6.4×10^{1}	4.3×10^{3}	1.2×10^{-16}
800	1050	1.0×10^{6}	3.6	3.5×10^{2}	2.7×10^{-17}

Table 8

Observed Ion Composition

Altitude (km)	Day (fractional abundance)			Night (fractional abundance)		
	O^+	O_2^+	NO^+	O^+	O_2^+	NO^+
100	0.00	0.40	0.60	0.00	0.00	1.00
150	0.10	0.25	0.65	0.05	0.30	0.65
200	0.65	0.10	0.25	0.35	0.25	0.40
250				0.85	0.05	0.05

Mass spectroscopic analysis of ion composition. The daytime measurements were made at 1207 CST, March 23, 1958; the nighttime measurements at 2321 CST, Nov. 20, 1956.

controlling process in determining composition.[3] The ionic compositions were measured by Johnson[4] using mass spectrometers mounted on rockets.

The kinetics of the ionization processes of the upper atmosphere are extremely interesting. The effective recombination coefficients in the various layers have been measured by radio reflection techniques during periods when the electron density changes appreciably, such as immediately after sunset or during a solar eclipse. An additional technique, particularly applicable to the E layer, involves the measurement of the "sluggishness" of the layer, the fact that the maximum electron density does not occur simultaneously with the maximum production rate. The result of these observations for the E and F_1 layers is that the effective recombination coefficient is large, and is almost independent of the gas or electron density. In contrast the effective recombination coefficient in the F_2 layer is moderate in magnitude, and is directly proportional to gas density and inversely proportional to electron density.[5] In order to explain these observations Bates and Massey[6] assumed that the ions in the E and F_1 layers are mainly molecular and devised the mechanism of dissociative recombination,

$$XY^+ + e \rightarrow X + Y \quad , \tag{58}$$

to account for the high rate of recombination. Since there is no analogue to dissociative recombination available to atomic ions, Bates[7] has suggested that atomic ions are first converted to molecular ions by a process of ion-atom interchange

$$Z^+ + XY \rightarrow ZX^+ + Y \tag{59}$$

and that dissociative recombination took place subsequently. On ascending through the F_2 layer, on the other hand, the frequency of ion-atom interchange collisions diminishes. In consequence, atomic ions would predominate in the upper part of the F_2 layer. The mass spectroscopic results bear out these general theoretical deductions with respect to ion composition of the ionosphere.

A. E Layer - Dissociative Recombination

Effective recombination coefficients in the E layer have been evaluated from several different processes and differing values have been obtained. In measurements of nocturnal recombination the effective recombination coefficient is found to decrease from about 10^{-8} to less than 10^{-9} cm^3/electrons sec as the night progresses. For the hours just after sunset, before the verticle motion of the layer affects the determination, Mitra[8] finds that the effective recombination coefficient has a mean value of 6.8×10^{-9} cm^3/electron sec with $n_e = 9 \times 10^3$ electrons/ cm^3. Measurements of the variation in electron density during a solar eclipse provide a second determination of recombination. It is commonly observed that the recombination coefficient is higher in the first stages of an eclipse than in the later stages. Typical values are 3×10^{-8} cm^3/ electrons sec in the initial stage and 5×10^{-9} cm^3/electrons sec in the final stage.[9] If it is assumed that the recombination coefficient is constant throughout the eclipse, the variation in its value may be attributed to a nonuniform distribution of the ionizing radiation over the sun's disk. This explanation leads to the awkward conclusion that the western limb of the sun is consistently brighter than the eastern. Alternatively the eclipse results may be explained in terms of the presence in the E layer of several ionic species with different rates of recombination. The value of the observed recombination coefficient then depends on the relative abundance of the various species. The value of α deduced from the initial phase of the eclipse would correspond to the relative abundance of these ions under normal daytime conditions. As the eclipse progresses, just as at night, the value of α decreases, reaching a minimum value in the final phase of the eclipse.[10, 11]

The coefficient for diurnal recombination is determined from measurements of the interval between the time of maximum electron production (local noon) and the time of maximum electron density in the layer. The recombination coefficient is related to the delay time t by the expression[12]

$$t = 1/2\alpha_s n_e \quad . \tag{60}$$

Values of α_s usually lie around 10^{-8} cm^3/electrons sec,[13] somewhat less than the value of α found from the initial phase of an eclipse. The discrepancy in the two values is predictable from the assumption that the E layer consists of a mixture of ions. By assuming that the layer consists of two ionic species, Bowhill[11] is able to account for the variance in the values of the effective recombination coefficients in a consistent manner. From his analysis he deduces the two specific recombination coefficients to be 6×10^{-8} and 6×10^{-9} cm^3/electron sec. On the basis of these values Bowhill estimates the relative concentration of the more rapidly recombining ion to be 0.47 in the day and 0.02 at night. By scaling the rocket data[4] in Table 8 to obtain the ion composition at an altitude of 110 km, the peak of the E layer, the rapidly recombining ion may be identified as O_2^+ and the other as NO^+ (see Table 5). On the basis of this identification, the estimated recombination coefficients for the reactions

$$O_2^+ + e \rightarrow O + O \tag{61}$$

$$NO^+ + e \rightarrow N + O \tag{62}$$

are 6×10^{-8} and 6×10^{-9} cm^3/electron sec, respectively.

Table 9

Relative Abundances of NO^+ and O_2^+ in the E Layer (110 km)

Ion	Day		Night	
	Measured	Calculated	Measured	Calculated
NO^+	0.73	0.53	0.97	0.98
O_2^+	0.27	0.47	0.03	0.02

B. F_2 Layer — Ion-Atom Interchange

As an ionized system the F_2 layer of the ionosphere differs considerably from the E layer, particularly in its ionization kinetics. In contrast to the E layer, atomic oxygen ions form an appreciable proportion of the ionization. The high relative abundance of O^+ together with the low particle density of the layer is primarily responsible for its characteristic recombination kinetics. Measurements of the electron loss rate at night reveal that recombination is much slower than in the E layer. The kinetic data obey a first order rate law, as though the electrons were lost by attachment, with an attachment coefficient that decreases with altitude.[5]

The apparent first-order kinetics might conceivably be explained in terms of radiative attachment followed by rapid ionic recombination:

$$O + e \rightarrow O^- + h\nu \qquad (63)$$

$$O^- + O^+ \rightarrow O + O \qquad (64)$$

(the concentration of O atoms remains effectively constant).

This mechanism was analyzed in detail by Bates and Massey[6] who concluded that the radiative attachment rate is not sufficiently rapid to account for the observed electron loss rate. Their arguments are strengthened by the subsequent determination that the electron affinity of atomic oxygen, instead of being 2.2 ev, is only 1.45 ev.[14]

In place of ionic recombination Bates and Massey proposed a recombination mechanism in which the atomic oxygen ions are first converted into molecular ions and then undergo dissociative recombination:

$$O^+ + XY \rightarrow O + XY^+ \tag{65}$$

$$XY^+ + e \rightarrow X + Y \quad . \tag{66}$$

They suggested that the conversion takes place through charge transfer, which requires that the molecule XY have a lower ionization potential than O^+. Both NO and O_2 satisfy this requirement, but N_2 does not.

Bates[7] has more recently questioned whether the change transfer process can be sufficiently effective in view of the fact that an electronic transition involving a considerable change in the internal energy is rarely brought about in a thermal collision. He suggests that the original mechanism be modified by replacing the first step with an ion-atom interchange process

$$O^+ + XY \rightarrow OX^+ + Y \quad . \tag{67}$$

An ion-atom interchange of this type does not necessitate an electronic change; consequently the limiting conditions of adiabatic encounters do not arise. Rather the process is essentially chemical in nature, taking place whenever the energy of relative motion exceeds an activation E_a, which may be a fraction of 1 ev. With ion-atom interchange XY may be NO, O_2 or N_2.

The combined mechanism of ion-atom interchange and dissociative recombination

$$O^+ + XY \rightarrow OX^+ + Y \tag{68}$$

$$OX^+ + e \rightarrow O + X \tag{69}$$

is consistent with the recombination rate data in the F layers. The effective rate of recombination depends on the slower of the two steps. In the F_1 layer, there are sufficient diatomic molecules present for ion-atom interchange to be a fairly fast process, but in the more rarefied F_2 layer this is not so and the effective recombination coefficient involves the ratio of diatomic molecule to electron concentration, which changes with height. The difference in recombination processes may be invoked to explain the splitting of the F layer into F_1 and F_2.

An order of magnitude estimate of the rate constant for ion-atom interchange is possible.[15] For O^+ four interchange reactions can be considered:

$$O^+ + N_2 \rightarrow NO^+ + N + 1.09 \text{ ev} \tag{70}$$

$$O^+ + O_2 \rightarrow O_2^+ + O + 1.53 \text{ ev} \tag{71}$$

$$O^+ + NO \rightarrow NO^+ + O + 4.36 \text{ ev} \tag{72}$$

$$O^+ + NO \rightarrow O_2^+ + N + 0.16 \text{ ev} \tag{73}$$

Since in the F_2 layer the concentrations of O^+ and electrons are almost equal, the rate of disappearance of O^+ during the night can be expressed by the experimental law for the rate of electron loss

$$\frac{d(O^+)}{dt} = - \beta (O^+) \quad . \tag{74}$$

The values of β determined by Ratcliffe[16] from radio data are 2.7×10^{-4}, 1.0×10^{-4}, and 3.7×10^{-5} sec^{-1} at 250, 300, and 350 km, respectively. Assuming that O^+ disappears by the interchange reactions (70) through (74), then

$$\frac{d(O^+)}{dt} = - \left\{ k_1 (N_2) + k_2 (O_2) + [k_3 + k_4] (NO) \right\} (O^+) \tag{75}$$

and

$$= k_1 (N_2) + k_2 (O_2) + [k_3 + k_4] (NO) \quad . \tag{76}$$

The NO^+ and O_2^+ formed by ion-atom interchange in turn undergo dissociative recombination; denoting the recombination coefficients for

$$O_2^+ + e \rightarrow O + O \tag{77}$$

$$NO^+ + e \rightarrow N + O \tag{78}$$

by α_1 and α_2, respectively, then during the night, when O_2^+ and NO^+ attain equilibrium,

$$\beta (O^+) = [\alpha_1 (O_2^+) + \alpha_2 (NO^+)] \, \eta_e \quad . \tag{79}$$

Since (O^+) and η_e are almost equal

$$\beta = \alpha_1 (NO^+) + \alpha_2 (O_2^+) \quad . \tag{80}$$

(Reactions (73) and (74) are neglected because of the very small concentration of NO in the F_2 layer.) If the values of α_1 and α_2 derived by Bowhill[11] from observations of the E layer, 6×10^{-8} and 6×10^{-9} cm^3/ion sec, are adopted for the F_2 layer (the temperature dependence of neither coefficient is known) and the concentrations of O_2^+ and NO^+ are taken as 7×10^3 ions/cm^3 on the basis of the relative abundances in Table 2 and the equilibrium night time electron density of 2.5×10^5, substitution of these estimates in (80) gives β to be 4×10^{-4}/sec at 250 km. The closeness of the agreement with the experimental result is somewhat fortuitous in view of the approximations employed, but the agreement lends credence to the mechanism of Bates and Massey.

Accepting the identification of the electron loss rate constant β with the over-all rate constant for ion-atom interchange, an order of magnitude estimate of the rate constants for the interchange O^+ with N_2 and O_2 reactions (70) and (71), can be made. Using the experimental value of β at 250 km and taking the concentrations of N_2 and O_2 to be as in Table 1, substitution into (76) (again neglecting terms involving NO) yields

$$k_1 + 0.09\, k_2 = 2.9 \times 10^{-13} \text{ cm}^3/\text{ion sec} \quad . \tag{81}$$

The recent laboratory determination by Sayers[17] of the O^+ - O_2 interchange reaction in oxygen afterglows yielded a rate constant of 2.5×10^{-11} cm^3/ion sec in the temperature range 200-300°K. No systematic temperature dependence was observed in this range. Other interchange studies, performed in the ion source of mass spectrometers, relate mainly to interchanges with hydrogen.[18] For these latter experiments the rate constants fell around the value of 10^{-9} cm^3/ion sec in reasonable agreement with a theory of Eyring[19] which assumes that all close encounters lead to interchange. However, adoption of a rate constant as high as 10^{-9} cm^3/ion sec for interchange in the ionosphere leads to erroneous predictions, such as that almost all the O^+ are replaced by NO^+ within a few seconds of sunset. That observed rate constants for interchange (except for cases involving hydrogen) are very much less than the value for close encounters suggests the presence of an activative energy. An important consequence is that k_1 and k_2 are likely to be rapidly increasing functions of the temperature. Refinements in observations, both in the ionosphere and the laboratory, are called for.

REFERENCES

1. G. V. Groves, "Nature," 184 178 (1959), Proc. Roy Soc. A263 212 (1961)

2. D. R. Bates, Proc. Ray Soc. A253 451 (1959)

3. M. Nicolet and P. Mange, J. Geophys. Res 59 15(1954)

4. C. Y. Johnson, E. B. Meadows, and J. C. Holmes, J. Geophys. Res. 63 443 (1958)

5. J. A. Ratcliff and K. Weeks in "Physics of the Upper Atmosphere," J. A. Ratcliffe (ed), Academic Press, New York (1960)

6. D. R. Bates and H. S. W. Massey, Proc. Roy Soc. A192 1(1947)

7. D. R. Bates, Proc. Phys. Soc. A68 344 (1955)

8. A. P. Mitra, J. Atmosph. Terr. Phys. 10 140 (1957)

9. J. A. Ratcliffe, "Solar Eclipses and the Ionosphere" (Suppl. to Vol 6, J. Atmosph. Terr Phys.) 1, Pergamon Press, London 1956.

10. M. W. McElhinny J. Atmosph. Terr. Phys. 14 273 (1959)

11. S. A. Bowhill, J. Atmosph. Terr. Phys. 20 19(1961)

12. E. V. Appleton, Proc. Roy Soc. A162 45d (1937)

13. E. V. Appleton, J. Atmosph. Terr. Phys. 3 282 (1953)

14. L. M. Branscomb and S. J. Smith, Phys. Rev 98 1127 (1955)
    F. M. Page, Trans. Fara. Soc. 57 359 (1961)

15. D. R. Bates and M. Nicolet, J. Atmosph. Terr. Phys. 18 65 (1960)

16. J. A. Ratcliffe, E. R. Schmerling, C. S. G. K. Setty and J. O. Thomas, Phil Trans. A248 621 (1956)

17. P. H. G. Dickinson and J. Sayers, Proc. Phys. Soc. (London) 137 (1960)

18. D. P. Stevenson and D. O. Schissler J. Chem. Phys. 29 282 (1958)

19. H. Eyring, J. O. Hirschfelder and H. S. Taylor, J. Chem. Phys. 4 479 (1936)

Aerospace Corporation, El Segundo, California. THE KINETICS OF IONIZATION PROCESSES IN GASES, prepared by Howard Myers. December 1961. [94] p. incl. illus.
(Report TDR-930(2119)TR-2)
(Contract AF 04(647)-930) Unclassified Report

Currently available knowledge of the kinetics of ionization is presented. The production of ionization is covered by a description of electrical discharges in gases, including direct and alternating current discharges. Photoionization and ionization by shock waves are described. The measurement of ionization includes a description of electrostatic probes, microwave probing signals, mass spectrometer probe and shock tubes. Photoionization instrumentation is described. Results of kinetic investigations are presented and the ionization processes occurring in the atmosphere are analyzed.

UNCLASSIFIED

UNCLASSIFIED

Aerospace Corporation, El Segundo, California. THE KINETICS OF IONIZATION PROCESSES IN GASES, prepared by Howard Myers. December 1961. [94] p. incl. illus.
(Report TDR-930(2119)TR-2)
(Contract AF 04(647)-930) Unclassified Report

Currently available knowledge of the kinetics of ionization is presented. The production of ionization is covered by a description of electrical discharges in gases, including direct and alternating current discharges. Photoionization and ionization by shock waves are described. The measurement of ionization includes a description of electrostatic probes, microwave probing signals, mass spectrometer probe and shock tubes. Photoionization instrumentation is described. Results of kinetic investigations are presented and the ionization processes occurring in the atmosphere are analyzed.

UNCLASSIFIED

UNCLASSIFIED

Aerospace Corporation, El Segundo, California. THE KINETICS OF IONIZATION PROCESSES IN GASES, prepared by Howard Myers. December 1961. [94] p. incl. illus.
(Report TDR-930(2119)TR-2)
(Contract AF 04(647)-930) Unclassified Report

Currently available knowledge of the kinetics of ionization is presented. The production of ionization is covered by a description of electrical discharges in gases, including direct and alternating current discharges. Photoionization and ionization by shock waves are described. The measurement of ionization includes a description of electrostatic probes, microwave probing signals, mass spectrometer probe and shock tubes. Photoionization instrumentation is described. Results of kinetic investigations are presented and the ionization processes occurring in the atmosphere are analyzed.

UNCLASSIFIED

UNCLASSIFIED

Aerospace Corporation, El Segundo, California. THE KINETICS OF IONIZATION PROCESSES IN GASES, prepared by Howard Myers. December 1961. [94] p. incl. illus.
(Report TDR-930(2119)TR-2)
(Contract AF 04(647)-930) Unclassified Report

Currently available knowledge of the kinetics of ionization is presented. The production of ionization is covered by a description of electrical discharges in gases, including direct and alternating current discharges. Photoionization and ionization by shock waves are described. The measurement of ionization includes a description of electrostatic probes, microwave probing signals, mass spectrometer probe and shock tubes. Photoionization instrumentation is described. Results of kinetic investigations are presented and the ionization processes occurring in the atmosphere are analyzed.

UNCLASSIFIED

UNCLASSIFIED

UNCLASSIFIED

UNCLASSIFIED

UNCLASSIFIED

UNCLASSIFIED

UNCLASSIFIED

UNCLASSIFIED

UNCLASSIFIED

UNCLASSIFIED